

# Theoretical aspects of Andreev spectroscopy and tunneling spectroscopy in non-centrosymmetric superconductors: a topical review

Matthias Eschrig, Christian Iniotakis, and Yukio Tanaka

**Abstract** Tunneling spectroscopy at surfaces of unconventional superconductors has proven an invaluable tool for obtaining information about the pairing symmetry. It is known that mid gap Andreev bound states manifest itself as a zero bias conductance peak in tunneling spectroscopy. The zero bias conductance peak is a signature for a non-trivial pair potential that exhibits different signs on different regions of the Fermi surface. Here, we review recent theoretical results on the spectrum of Andreev bound states near interfaces and surfaces in non-centrosymmetric superconductors. We introduce a theoretical scheme to calculate the energy spectrum of a non-centrosymmetric superconductor. Then, we discuss the interplay between the spin orbit vector field on the Fermi surface and the order parameter symmetry. The Andreev states carry a spin supercurrent and represent a helical edge mode along the interface. We study the topological nature of the resulting edge currents. If the triplet component of the order parameter dominates, then the helical edge mode exists. If, on the other hand, the singlet component dominates, the helical edge mode is absent. A quantum phase transition occurs for equal spin singlet and triplet order parameter components. We discuss the tunneling conductance and the Andreev point contact conductance between a normal metal and a non-centrosymmetric superconductor.

---

Matthias Eschrig

(a) Fachbereich Physik, Universität Konstanz, D-78464 Konstanz, Germany, and

(b) Institut für Theoretische Festkörperphysik and DFG-Center for Functional Nanostructures, Karlsruhe Institute of Technology D-76128 Karlsruhe, Germany,

e-mail: Matthias.Eschrig@kit.de

Christian Iniotakis

Institute for Theoretical Physics, ETH Zurich, 8093 Zurich, Switzerland,

e-mail: iniotaki@phys.ethz.ch

Yukio Tanaka

Department of Applied Physics, Nagoya University, Nagoya, 464-8603, Japan

e-mail: ytanaka@nuap.nagoya-u.ac.jp

## 1 Introduction

In this chapter, we will discuss the surface and interface properties of non-centrosymmetric superconductors [35] focusing on the tunneling conductance. Since the early sixties tunneling spectroscopy has played an important role in gathering information about the gap function of conventional superconductors [1]. In the context of unconventional superconductivity tunneling spectroscopy appeared as an important tool to probe the internal phase structure of the Cooper pair wave functions [2, 3]. Surface states with sub-gap energy, known as Andreev bound states (ABS) [4–7] provide channels for resonant tunneling leading to so-called zero-bias anomalies in  $dI/dV$ . Zero-bias anomalies observed in high-temperature superconductors showed the presence of zero-energy bound states at the surface, giving strong evidence for  $d$ -wave pairing [2–6]. Similarly the tunneling spectrum observed in  $\text{Sr}_2\text{RuO}_4$  is consistent with the existence of chiral surface states as expected for a chiral  $p$ -wave superconductor [8–10]. Zero bias conductance peaks due to Andreev bound states have been observed in numerous experiments, e.g. in high- $T_c$  cuprates [11],  $\text{Sr}_2\text{RuO}_4$  [12, 13],  $\text{UBe}_{13}$  [14],  $\text{CeCoIn}_5$  [15], the two dimensional organic superconductor  $\kappa$ -(BEDT-TTF) $_2\text{Cu}[\text{N}(\text{CN})_2]\text{Br}$  [16] and  $\text{PrOs}_4\text{Sb}_{12}$  [17]. Andreev bound states have also been observed in the Balian-Werthammer phase of superfluid  $^3\text{He}$  [18]. The study of Andreev bound states in unconventional superconductors and superfluids has emerged as an important phase sensitive probe.

In section 2 we present the theory for Andreev spectroscopy using Bogoliubov wave function technique in Andreev approximation. Starting with superconductors exhibiting  $d$ -wave or  $p$ -wave pairing, we proceed with non-centrosymmetric superconductors. In section 3, we develop the theoretical tools for describing Andreev spectroscopy in non-centrosymmetric superconductors in the framework of Nambu-Gor'kov Green's functions within the quasiclassical theory of superconductivity.

## 2 Andreev spectroscopy in unconventional superconductors

### 2.1 Andreev conductance in $s$ - and $d$ -wave superconductors

We discuss first the example of zero-bias resonant states at the interface of a normal metal/spin-singlet  $d$ -wave superconductor junction. In general, the pair potential can be expressed in terms of two coordinates,  $\mathbf{x}$  and  $\mathbf{x}'$ , as  $\Delta(\mathbf{x}, \mathbf{x}')$ . In uniform systems it only depends on the relative coordinate  $\mathbf{x} - \mathbf{x}'$ , and a Fourier transform with respect to it yields  $\Delta(\mathbf{k})$  with relative momentum  $\mathbf{k}$ . For illustrative purposes, we assume in the following a cylindrical Fermi surface and concentrate on two-dimensional systems. The pair potential for spin-singlet  $d$ -wave pairing is  $\Delta(\theta) = \Delta_0 \cos(2\theta)$ , with  $e^{i\theta} = (k_x + ik_y)/|\mathbf{k}|$ , while the corresponding spin-singlet  $s$ -wave one is isotropic,  $\Delta(\theta) = \Delta_0$ . The bulk quasiparticle density of states normalized by its value in the normal state is given by

$$\rho_B(E) = \frac{1}{\pi} \int_0^\pi d\theta \rho_0(E, \Delta(\theta)), \quad \rho_0(E, \Delta(\theta)) = \frac{E}{\sqrt{E^2 - \Delta_0^2 \cos^2(2\theta)}}. \quad (1)$$

For a spin-singlet  $d$ -wave superconductor this quantity behaves linearly at low energies,  $\rho(E) \propto |E|$ . As shown below if the angle between the interface normal and the lobe direction of the  $d$ -wave pair potential has a nonzero value  $\alpha$  with  $0 < \alpha < \pi/2$ , then the resulting tunneling conductance  $\sigma_T(E)$  has a zero bias conductance peak.

The Andreev conductance for a normal metal/insulator/spin singlet  $s$ -wave superconductor junction is described by the model of Blonder, Tinkham, and Klapwijk (BTK) [19]. Within this model,  $\sigma_T(E)$  at zero temperature is given by

$$\sigma_T(E) \propto \sum_\theta (1 + |a(E, \theta)|^2 - |b(E, \theta)|^2) \quad (2)$$

where  $a(E, \theta)$ , and  $b(E, \theta)$  are probability amplitude coefficients for Andreev reflection and for normal reflection, respectively. We apply the BTK model in the following to the case of spin-singlet  $d$ -wave pairing.

We assume that the Fermi energy  $E_F$  is much larger than  $|\Delta(\theta)|$ , such that the Andreev approximation can be applied to the Bogoliubov wave functions. For simplicity, we also assume equal effective masses and Fermi momenta in the normal metal and in the superconductor. The spatial dependence of the pair potential is chosen to be  $\Delta(\theta)\Theta(x)$  (with the Heaviside step function  $\Theta$ ). The insulating barrier at the atomically clean interface is modeled by a  $\delta$ -function potential,  $V(x) = H\delta(x)$ . Since the momentum parallel to the interface is conserved, the two component Bogoliubov wave function is given in Andreev approximation by

$$\Psi(\theta, x) = \begin{pmatrix} u_+(\theta, x) \\ v_+(\theta, x) \end{pmatrix} \exp(ik_F x \cos \theta) + \begin{pmatrix} u_-(\theta, x) \\ v_-(\theta, x) \end{pmatrix} \exp(-ik_F x \cos \theta) \quad (3)$$

where  $u_j(\theta, x)$  and  $v_j(\theta, x)$  with  $(j = +, -)$  obey the Andreev equations

$$\begin{aligned} Eu_j(\theta, x) &= - \left[ \frac{i\hbar^2 \sigma_j k_F \cos \theta}{m} \frac{d}{dx} - H\delta(x) \right] u_j(\theta, x) + \Delta(\theta_j)\Theta(x)v_j(\theta, x), \\ Ev_j(\theta, x) &= \left[ \frac{i\hbar^2 \sigma_j k_F \cos \theta}{m} \frac{d}{dx} - H\delta(x) \right] v_j(\theta, x) + \Delta^*(\theta_j)\Theta(x)u_j(\theta, x), \end{aligned} \quad (4)$$

with  $\sigma_+ = 1$ ,  $\theta_+ = \theta$ , and  $\sigma_- = -1$ ,  $\theta_- = \pi - \theta$ . For a  $d$ -wave superconductor the corresponding effective pair potentials  $\Delta(\theta_\pm)$  are given by

$$\Delta(\theta_+) = \Delta_0 \cos(2\theta - 2\alpha), \quad \Delta(\theta_-) = \Delta_0 \cos(2\theta + 2\alpha), \quad (5)$$

where the angle between the interface normal and the lobe direction of the  $d$ -wave pair is  $\alpha$ . The wave functions  $u_\pm(\theta, x)$  and  $v_\pm(\theta, x)$  resulting from Eqs. (4) are obtained from by ansatz

$$\begin{pmatrix} u_+(\theta, x) \\ v_+(\theta, x) \end{pmatrix} = \begin{cases} \begin{pmatrix} 1 \\ 0 \end{pmatrix} \exp(i\delta x) + a(E, \theta) \begin{pmatrix} 0 \\ 1 \end{pmatrix} \exp(-i\delta x) & x < 0 \\ c(E, \theta) \begin{pmatrix} \sqrt{(E + \Omega_+)/2E} \\ \exp(-i\phi_+) \sqrt{(E - \Omega_+)/2E} \end{pmatrix} \exp(i\gamma_+ x) & x > 0 \end{cases}, \quad (6)$$

$$\begin{pmatrix} u_-(\theta, x) \\ v_-(\theta, x) \end{pmatrix} = \begin{cases} b(E, \theta) \begin{pmatrix} 1 \\ 0 \end{pmatrix} \exp(-i\delta x) & x < 0 \\ d(E, \theta) \begin{pmatrix} \exp(i\phi_-) \sqrt{(E - \Omega_-)/2E} \\ \sqrt{(E + \Omega_-)/2E} \end{pmatrix} \exp(i\gamma_- x) & x > 0 \end{cases} \quad (7)$$

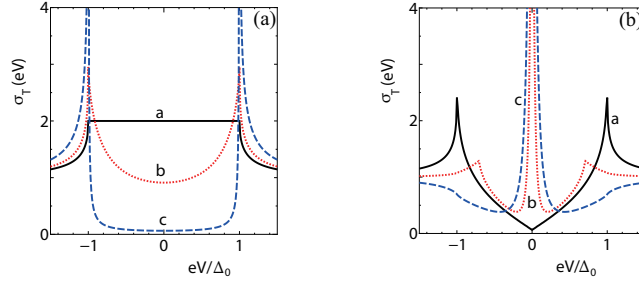


**Fig. 1** (Color online) Left: Tunneling conductance for an *s*-wave superconductor. a:  $Z = 0$ , b:  $Z = 1$  and c:  $Z = 5$ . Right: Tunneling conductance for a *d*-wave superconductor for  $Z = 5$ . a:  $\alpha = 0$ , b:  $\alpha = 0.125\pi$  and c:  $\alpha = 0.25\pi$ .

where we used the abbreviations

$$\delta = \frac{Em}{\hbar k_F \cos \theta}, \quad \gamma_{\pm} = \frac{\Omega_{\pm} m}{\hbar k_F \cos \theta}, \quad \Omega_{\pm} = \sqrt{E^2 - \Delta^2(\theta_{\pm})}, \quad \exp(i\phi_{\pm}) = \frac{\Delta(\theta_{\pm})}{|\Delta(\theta_{\pm})|}. \quad (8)$$

With the help of appropriate boundary conditions,

$$\begin{aligned} \Psi(\theta, x)|_{x=0_-} &= \Psi(\theta, x)|_{x=0_+} \\ \frac{d}{dx} \Psi(\theta, x)|_{x=0_+} - \frac{d}{dx} \Psi(\theta, x)|_{x=0_-} &= \frac{2mH}{\hbar^2} \Psi(\theta, x)|_{x=0_+} \end{aligned} \quad (9)$$

we obtain  $a(E, \theta)$ ,  $b(E, \theta)$ ,  $c(E, \theta)$ , and  $d(E, \theta)$ .

The resulting conductance is

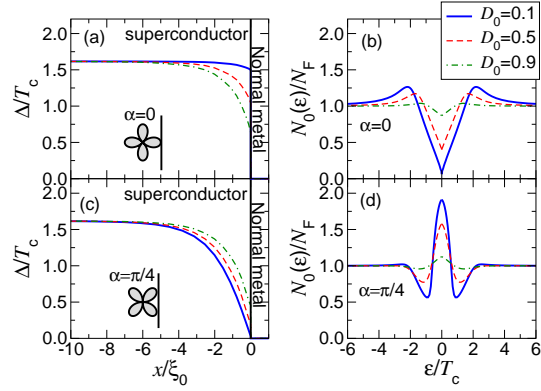
$$\begin{aligned} \sigma_T(E) &= \left( \int_{-\pi/2}^{\pi/2} d\theta D(\theta) \sigma_R(E, \theta) \cos \theta \right) / \left( \int_{-\pi/2}^{\pi/2} d\theta D(\theta) \cos \theta \right), \\ \sigma_R(E, \theta) &= \frac{1 + D(\theta) |\Gamma_+|^2 - R(\theta) |\Gamma_+ \Gamma_-|^2}{|1 - R(\theta) \Gamma_+ \Gamma_- \exp[i(\phi_- - \phi_+)]|^2}, \end{aligned} \quad (10)$$

with  $\Gamma_{\pm} = (E - \Omega_{\pm}) / |\Delta(\theta_{\pm})|$ . The quantities  $D(\theta)$  and  $R(\theta)$  above are given by

$$D(\theta) = 4 \cos^2 \theta / (4 \cos^2 \theta + Z^2), \quad R(\theta) = 1 - D(\theta),$$

with injection angle  $\theta$  and  $Z = 2mH/\hbar^2 k_F$  [2]. Choosing  $\Delta(\theta_{\pm}) = \Delta_0$  reproduces the BTK formula for an *s*-wave superconductor. Typical line shapes of  $\sigma_T(eV)$  with  $eV = E$  for *s*-wave and *d*-wave superconductors are shown in Fig. 1. The *d*-wave case is shown in Fig. 1(b). As can be seen there, if the angle  $\alpha$  deviates from 0, the resulting  $dI/dV$  has a zero bias conduction peak (ZBCP) (curves b and c); the only exceptional case is  $\alpha = 0$ , as shown in curve a. The width of the ZBCP is proportional to  $D$ , while its height is proportional to the inverse of  $D$ . The origin of this peak are mid gap Andreev bound states (MABS). The condition of the formation for Andreev bound states at the surface of an isolated *d*-wave superconductor ( $D \rightarrow$

**Fig. 2** (a)+(c): order parameter amplitude and (b)+(d): local density of states at the interface for a layered  $d$ -wave-superconductor/normal-metal junction. (a)+(b):  $\alpha = 0$ , (c)+(d):  $\alpha = \pi/4$ . The interface is at  $x = 0$ . The curves are for the indicated transmission coefficients  $D_0$ . The temperature is  $T = 0.3T_c$ , and the mean free path  $\ell = 10\xi_0$ . After Ref. [20].



0) is expressed by

$$1 = \Gamma_+ \Gamma_- \exp[i(\phi_- - \phi_+)]. \quad (11)$$

At zero energy  $\Gamma_+ \Gamma_- = -1$  is satisfied, and consequently a MABS appears provided  $\exp[i(\phi_+ - \phi_-)] = -1$ . For this case, on the superconducting side of the interface, the injected electron and the reflected hole experience a different sign of the pair potential. For  $\alpha = \pi/4$ , there is a MABS independent of the injection angle. In this case, the energy dispersion of the resulting ABS,  $E_b$ , is given by

$$E_b = 0. \quad (12)$$

Finally, we comment on the effects of order parameter suppression near an surface or interface in a  $d$ -wave superconductor. In Fig. 2 we reproduce a self-consistent solution for a layered  $d$ -wave superconductor, showing that a strong order parameter suppression is always present for  $\alpha = 0.25$ , whereas for  $\alpha = 0$  in the tunneling limit the order parameter suppression can be neglected. The corresponding local density of states at the surface is shown in Fig. 2(b) and (d). The interface is modeled by a  $\delta$ -potential as above, with a transmission  $D(\theta) = D_0 \cos^2 \theta / (1 - D_0 \sin^2 \theta)$ , and the parameter  $D_0$  is related to  $Z$  via  $D_0 = 1/[1 + (Z/2)^2]$ .

## 2.2 Andreev conductance in chiral $p$ -wave superconductor

In this section, we discuss the tunneling conductance of a normal metal/chiral  $p$ -wave superconductor junction. There is evidence supporting the realization of spin-triplet pairing with broken time reversal symmetry in the superconducting state of  $\text{Sr}_2\text{RuO}_4$  [21–26]. A possible symmetry is given by two-dimensional chiral  $p$ -wave pairing, where the pair potentials are given by  $\Delta_{\uparrow,\uparrow} = \Delta_{\downarrow,\downarrow} = 0$ ,  $\Delta_{\uparrow,\downarrow} = \Delta_{\downarrow,\uparrow} = \Delta_0 \exp(i\theta)$ . In the following,  $\theta$  is measured from the interface normal. In the actual sample, the presence of chirality may produce chiral domain structures. A recent experiment is consistent with the presence of chiral domains [27]. Also, there are

several theoretical proposals to detect chiral domain structures [28]. Here, for simplicity, we consider a single domain chiral  $p$ -wave superconductor.

Since the  $z$ -component of the Cooper pair spin is zero, we can also use Eq. (10) to obtain the tunneling conductance for normal metal/chiral  $p$ -wave superconductor junctions. Before discussing the tunneling conductance, we first consider the bulk local density of states (LDOS) of a chiral  $p$ -wave superconductor. In contrast to the spin-singlet  $d$ -wave pairing case,  $\rho_0(E, \Delta(\theta))$  in Eq. (1) is given by

$$\rho_0(E, \Delta(\theta)) = E / \sqrt{E^2 - \Delta_0^2}.$$

It has a fully gapped density of state like in the spin-singlet  $s$ -wave case.

We now discuss the condition when an ABS is formed at the surface of an isolated chiral  $p$ -wave superconductor. The bound state condition is given by [8, 9]

$$E + \sqrt{E^2 - \Delta_0^2} = - \left( E - \sqrt{E^2 - \Delta_0^2} \right) \exp(-2i\theta), \quad (13)$$

showing that the bound state level  $E_b$  satisfies

$$E_b(\theta) = \Delta_0 \sin \theta \quad (14)$$

Note that the ABS has a dispersion different from that in the  $d$ -wave case with  $\alpha = \pi/4$ . The presence of the edge state with a dispersion induces a spontaneous dissipationless current.

As in the previous section we consider the tunneling conductance  $\sigma_T(E)$  in a normal metal/chiral  $p$ -wave superconductor junction, which is shown in Fig. 3(a). As can be seen, for  $Z = 0$ , the line shape of conductance is identical to that of a spin-singlet  $s$ -wave superconductor (see curve  $a$ ), whereas with increasing  $Z$  a zero bias conductance peak emerges (curves  $b$  and  $c$ ). The resulting ZBCP is broad in contrast to the spin-singlet  $d$ -wave case due to the fact that the position of the ABS

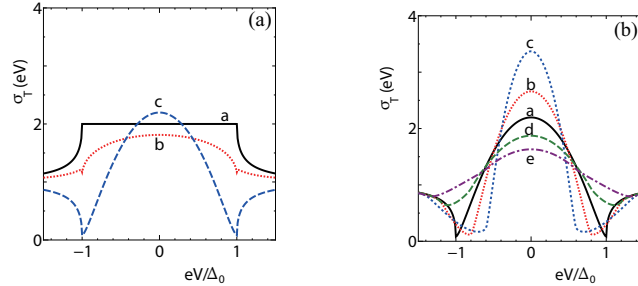


**Fig. 3** (Color online) (a): Tunneling conductance for a chiral  $p$ -wave superconductor. a:  $Z = 0$ , b:  $Z = 1$  and c:  $Z = 5$ . (b): Tunneling conductance for a chiral  $p$ -wave superconductor in the presence of a magnetic field for  $Z = 0$ . a:  $H = 0$ , b:  $H = 0.2H_0$  and c:  $H = 0.4H_0$ , d:  $H = -0.2H_0$  and e:  $H = -0.4H_0$ .

depends on the injection angle  $\theta$  according to Eq. (14) [8]. The presence of the ABS has been confirmed by tunneling experiments [12, 13].

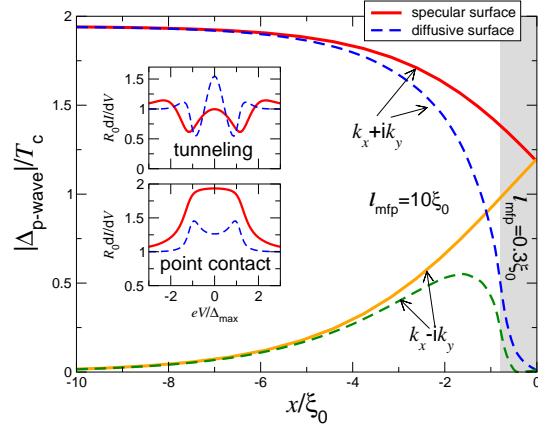
Next we consider the situation where a magnetic field  $H$  is applied perpendicular to the two-dimensional plane, which induces a shielding current along the interface. When the penetration depth for the chiral  $p$ -wave superconducting material is much longer than the coherence length, the vector potential can be approximated as  $\mathbf{A}(\mathbf{r}) = (0, A_y(x), 0)$  with  $A_y(x) = -\lambda_m H \exp(-x/\lambda_m)$ , where  $\lambda_m$  is the penetration depth. In the following we consider the situation where Landau level quantization can be neglected. Then the quasiclassical approximation can be used. The applied magnetic field shifts the quasiparticle energy  $E$  to  $E + H\Delta_0 \sin\phi/H_0$  with  $H_0 = h/(2e\pi^2\xi\lambda_m)$  and  $\xi = \hbar^2 k_F/(\pi m\Delta_0)$  [29]. The resulting tunneling conductance for various magnetic fields is plotted in Fig. 3(b). As is seen,  $\sigma_T(E)$  is enhanced for positive  $H$ , while it is reduced for negative  $H$ . This can be roughly understood by looking at the bound state levels. In the presence of  $H$ , the bound state energy can be expressed by

$$E_b(\theta) = \Delta_0(1 - H/H_0) \sin\theta \sim \Delta_0(1 - H/H_0)k_y/k_F. \quad (15)$$

The contribution of the Andreev bound state to the conductance enters via a term  $\delta(E - E_b(\theta))$ , which is proportional to  $1/|dE_b(\theta)/d\theta|$ . It is clear that the slope of the dispersion around  $\theta = 0$  is reduced for positive  $H$ , leading to an enhancement of the numerator in Eq. 10 around  $\theta = 0$ , where the bound states are close to zero energy. On the other hand, for negative  $H$ , the height of the ZBCP is reduced since the slope of the curve of  $E_b$  around zero energy becomes steeper [10].

In  $p$ -wave superconductors self-consistency of the order parameter and impurity effects can be of importance. In Fig. 4 we show self-consistent order parameters and Andreev spectra at a surface of a layered  $p$ -wave superconductor. In addition to the bulk  $k_x + ik_y$  component a subdominant  $k_x - ik_y$  component is stabilized within a few coherence lengths ( $\xi_0 = v_F/2\pi k_B T_c$ ) near the surface. The full lines are results assuming a mean free path of  $\ell = 10\xi_0$  everywhere. When replacing the mean free

**Fig. 4** (Color online) Self-consistent order parameter near a surface of a layered  $p$ -wave superconductor. Full lines are for mean free path  $\ell_{\text{mfp}} = 10\xi_0$  everywhere; dashed lines are for a shortened  $\ell_{\text{mfp}} = 0.3\xi_0$  in the gray shaded region. The calculations are for  $T = 0.1T_c$ . Insets: point contact spectra for fully transparent interface (bottom) and tunneling conductance ( $D_0 = 0.05$ ) (top). After Ref. [30].



path in a surface layer (gray shaded region in Fig. 4) by  $\ell = 0.3\xi_0$ , we obtain the results shown as dashed lines. In contrast to the first case, for the second case both order parameter components are strongly suppressed near the surface. The presence of an increased scattering in a surface layer also modifies the form of point contact spectra and the tunneling conductance as seen in the insets of Fig. 4. In contrast to the surface density of states which for a clean surface is constant in energy, the tunneling conductance shows a broad peak similar as in Fig. 3, which is however reduced in height for a self consistent order parameter [31].

Finally, we would like to comment that the above edge state is topologically equivalent to that of a quantum Hall system. In a quantum Hall system it is established that the edge channel supports the accurate quantization of the Hall conductance  $\sigma_H$ , which is related to a topological integer [32, 33]. In the edge state of a chiral  $p$ -wave superconductor, such a topological number can be also defined [34]. For this case, the edge state is topologically protected by the bulk energy gap  $\Delta_0$ . The topological properties of the electronic states have been attracting intensive interest in condensed matter physics. In section 2.3.3 we will return to this question in connection with non-centrosymmetric superconductors. Before that, we discuss in the following section theoretical predictions for the Andreev conductance spectra for non-centrosymmetric superconductors.

### 2.3 Andreev conductance in non-centrosymmetric superconductors

Non-centrosymmetric superconductors such as CePt<sub>3</sub>Si are a central topic of current research [35, 36]. Two-dimensional non-centrosymmetric superconductors are expected e.g. at interfaces and/or surfaces due to a strong potential gradient. An interesting example is superconductivity at a LaAlO<sub>3</sub>/SrTiO<sub>3</sub> interface [37, 38]. In non-centrosymmetric materials spin-orbit interaction becomes very important. Frigeri et al. [36] have shown that the  $(p_x \pm ip_y)$ -pairing state has the highest  $T_c$  within the triplet-channel in CePt<sub>3</sub>Si. It has been shown that singlet ( $s$ -wave) and triplet ( $p$ -wave) pairing is mixed, and several novel properties related to that mixing, such as a large upper critical field beyond the Pauli limit, have been focused on [36]. On the other hand, a pure  $(p_x \pm ip_y)$ -pairing state has been studied as a superconducting analogue of a quantum spin Hall system [39]. Therefore, it is an important and urgent issue to study the spin transport properties of the NCS superconductors from a topological viewpoint.

In this section, we discuss charge and spin transport in non-centrosymmetric superconductors [40]. We concentrate on non-centrosymmetric superconductors with time-reversal symmetry, where a spin-triplet  $(p_x \pm ip_y)$ -wave and a spin-singlet  $s$ -wave pair potential can mix with each other, similar as discussed in the last section. We show that when the amplitude of the  $(p_x \pm ip_y)$ -wave component is larger than that of the  $s$ -wave component, then the superconducting state belongs to a topologically nontrivial class analogous to a quantum spin Hall system, and the resulting helical edge modes are spin current carrying Andreev bound states that are topo-



logically protected. Below, we study Andreev reflection [41] at low energy, which is determined mostly by the helical edge modes, and find the spin polarized current flowing through an interface as a function of incident angle. When a magnetic field is applied, even the angle-integrated current is spin polarized.

### 2.3.1 Andreev bound states

We start with the Hamiltonian of a non-centrosymmetric superconductor

$$\hat{\mathcal{H}}_S = \begin{pmatrix} H(\mathbf{k}) & \Delta(\mathbf{k}) \\ -\Delta^*(-\mathbf{k}) & -H^*(-\mathbf{k}) \end{pmatrix}$$

with  $H(\mathbf{k}) = \xi_{\mathbf{k}} + \mathbf{g}(\mathbf{k}) \cdot \boldsymbol{\sigma}$ ,  $\mathbf{g}(\mathbf{k}) = \lambda(\hat{x}k_y - \hat{y}k_x)$ ,  $\xi_{\mathbf{k}} = \hbar^2 \mathbf{k}^2 / (2m) - \mu$ . Here,  $\mu$ ,  $m$ ,  $\boldsymbol{\sigma}$  and  $\lambda$  denote chemical potential, effective mass, Pauli matrices and coupling constant of Rashba spin-orbit interaction, respectively [36]. The pair potential  $\Delta(\mathbf{k})$  is given by

$$\Delta(\mathbf{k}) = [\mathbf{d}(\mathbf{k}) \cdot \boldsymbol{\sigma} + \psi(\mathbf{k})]i\sigma_y. \quad (16)$$

We choose  $(p_x \pm ip_y)$  with  $\mathbf{d}(\mathbf{k}) = \Delta_p(\hat{x}k_y - \hat{y}k_x) / |\mathbf{k}|$  for the spin-triplet component [36], and  $\psi(\mathbf{k}) = \Delta_s$  with  $\Delta_p \geq 0$  and  $\Delta_s \geq 0$ . The superconducting gaps  $\Delta_1 = \Delta_p + \Delta_s$  and  $\Delta_2 = |\Delta_p - \Delta_s|$  open for the two spin-split energy bands, respectively, in the homogeneous state [42]. As we will show below, surface states are crucially influenced by the relative magnitude between  $\Delta_p$  and  $\Delta_s$ .

Let us consider the wave functions, focusing on those for ABS localized at the surface. Consider a two-dimensional semi-infinite superconductor for  $x > 0$  where the surface is located at  $x = 0$ . The corresponding wave function is given by [43]

$$\Psi_S(x) = e^{ik_y y} \left[ c_1 \psi_1 e^{iq_{1x}^+ x} + c_2 \psi_2 e^{-iq_{1x}^- x} + c_3 \psi_3 e^{iq_{2x}^+ x} + c_4 \psi_4 e^{-iq_{2x}^- x} \right],$$

$$q_{jx}^{\pm} = k_{jx}^{\pm} \pm (k_j / k_{jx}^{\pm}) \sqrt{(E^2 - \Delta_j^2) / (\lambda^2 + 2\hbar^2 \mu / m)}, \quad (17)$$

with  $j = \{1, 2\}$ , and  $k_{jx}^+ = k_{jx}^- = k_{jx}$  for  $|k_y| \leq k_j$  and  $k_{jx}^+ = -k_{jx}^- = k_{jx}$  for  $|k_y| > k_j$ . Here,  $k_1$  and  $k_2$  with

$$k_{1(2)} = \mp m\lambda / \hbar^2 + \sqrt{(m\lambda / \hbar^2)^2 + 2m\mu / \hbar^2} \quad (18)$$

are the Fermi momenta of the small and large Fermi surface, respectively (the upper sign holds for  $k_1$ ), and  $k_{jx}$  denotes the  $x$  component of the Fermi momentum  $k_j$ , with  $k_{jx} = \sqrt{k_j^2 - k_y^2}$ . The wave functions are given by

$$\psi_1 = \begin{pmatrix} u_1 \\ -i\alpha_1^{-1}u_1 \\ i\alpha_1^{-1}v_1 \\ v_1 \end{pmatrix}, \psi_2 = \begin{pmatrix} v_1 \\ -i\tilde{\alpha}_1^{-1}v_1 \\ i\tilde{\alpha}_1^{-1}u_1 \\ u_1 \end{pmatrix}, \psi_3 = \begin{pmatrix} u_2 \\ i\alpha_2^{-1}u_2 \\ i\gamma\alpha_2^{-1}v_2 \\ -\gamma v_2 \end{pmatrix}, \psi_4 = \begin{pmatrix} v_2 \\ i\tilde{\alpha}_2^{-1}v_2 \\ i\gamma\tilde{\alpha}_2^{-1}u_2 \\ -\gamma u_2 \end{pmatrix}$$

with  $\gamma = \text{sgn}(\Delta_p - \Delta_s)$ . In the above,

$$u_j = \sqrt{(E + \sqrt{E^2 - \Delta_j^2}) / 2E}, \quad v_j = \sqrt{(E - \sqrt{E^2 - \Delta_j^2}) / 2E}. \quad (19)$$

Here we have introduced  $\alpha_1 = (k_{1x}^+ - ik_y)/k_1$ ,  $\alpha_2 = (k_{2x}^+ - ik_y)/k_2$ ,  $\tilde{\alpha}_1 = (-k_{1x}^- - ik_y)/k_1$ , and  $\tilde{\alpha}_2 = (-k_{2x}^- - ik_y)/k_2$ .  $E$  is the quasiparticle energy measured from the Fermi energy. By postulating  $\Psi_S(x) = 0$  at  $x = 0$ , we can determine the ABS.

The bound state condition can be expressed by

$$\sqrt{(\Delta_1^2 - E^2)(\Delta_2^2 - E^2)} = \frac{1 - \zeta}{1 + \zeta}(E^2 + \gamma\Delta_1\Delta_2), \quad (20)$$

$$\zeta = \begin{cases} \frac{\sin^2[\frac{1}{2}(\theta_1 + \theta_2)]}{\cos^2[\frac{1}{2}(\theta_1 - \theta_2)]} & \text{for } |\theta_2| \leq \theta_c \\ 1 & \text{for } \theta_c < |\theta_2| \leq \pi/2, \end{cases} \quad (21)$$

with  $\zeta \leq 1$ ,  $\cos \theta_1 = k_{1x}/k_1$  and  $\cos \theta_2 = k_{2x}/k_2$ . The critical angle  $\theta_c$  is defined as  $\arcsin(k_1/k_2)$ . For  $\lambda = 0$ , Eq. (20) reproduces the previous results [42]. As seen from Eq. (20), a zero energy ABS is only possible for  $|\theta_2| \leq \theta_c$  and  $\gamma = 1$ , i.e.  $\Delta_p > \Delta_s$ . This ABS corresponds to a state in which a localized quasiparticle can move along the edge. The energy level of this edge state depends crucially on the direction of the motion of the quasiparticle. The inner gap edge modes are absent for large magnitude of  $k_y$ , i.e.  $\theta_2$ . In this case,  $k_{1x}$  becomes a purely imaginary number due to the conservation of the Fermi momentum component parallel to the surface. The parameter regime where the edge modes survive is reduced with increasing  $\lambda$ . However, as far as we concentrate on normal injection, the edge modes survive as midgap ABS [2, 5] irrespective of the strength of  $\lambda$ . If we focus on the low energy limit, the ABS energy can be written as

$$E = \pm \Delta_p \left( 1 - \frac{\Delta_s^2}{\Delta_p^2} \right) \frac{k_1 + k_2}{2k_1k_2} k_y, \quad (22)$$

with  $\Delta_s < \Delta_p$  for any  $\lambda$  with small magnitude of  $k_y$ . For  $\Delta_s \geq \Delta_p$ , the ABS vanishes since the value of right hand side of Eq. (20) becomes negative, due to the negative sign of  $\gamma$  for  $|E| < \Delta_1$  and  $|E| < \Delta_2$ . It should be remarked that the ABS under consideration does not break time reversal symmetry, since the edge currents carried by the two partners of the Kramers doublet flow in opposite directions. Thus they can be regarded as helical edge modes, with the two modes related to each other by a time reversal operation.

### 2.3.2 Charge and spin conductance

Now we turn to transport properties governed by the ABS in NCS superconductors [44–46]. First, we point out that the spin Hall effect, i.e., the appearance of the spin Hall voltage perpendicular to the superconducting current, is suppressed by the compressive nature of the superconducting state by the factor of  $(k_F\lambda_m)^{-2}$  ( $k_F$ : Fermi momentum,  $\lambda_m$ : penetration depth) [34]. Instead, we will show below that spin transport through the junction between a ballistic normal metal at  $x < 0$  and a NCS superconductor, i.e., through a N/NSC junction, can be enhanced by

the Doppler effect during Andreev reflection. The Hamiltonian  $\mathcal{H}_N$  of N is given by putting  $\Delta(\mathbf{k}) = 0$  and  $\lambda = 0$  in  $\mathcal{H}_S$ . We assume an insulating barrier at  $x = 0$ , expressed by a delta-function potential  $U\delta(x)$ .

The quantities of interest are the angle resolved spin conductance  $f_S(\theta)$  and charge conductance  $f_C(\theta)$  defined by [47]

$$f_S(\theta) = \frac{1}{2} \left[ \sum_{\sigma,\rho} s_\rho (|a_{\sigma,\rho}|^2 - |b_{\sigma,\rho}|^2) \right] \cos \theta, \quad (23)$$

$$f_C(\theta) = \left[ 1 + \frac{1}{2} \sum_{\sigma,\rho} (|a_{\sigma,\rho}|^2 - |b_{\sigma,\rho}|^2) \right] \cos \theta, \quad (24)$$

where  $s_\rho = +(-)1$  for  $\rho = \uparrow (\downarrow)$ , and  $\theta$  denotes the injection angle measured from the normal to the interface. Here,  $b_{\sigma,\rho}$  and  $a_{\sigma,\rho}$  with  $\sigma, \rho \in \{\uparrow, \downarrow\}$  are spin-dependent reflection and Andreev reflection coefficients, respectively.

These coefficients are determined as follows. The wave function for spin  $\sigma$  in the normal metal  $\Psi_N(x)$  is given by

$$\Psi_N(x) = \exp(ik_F y) \left[ (\psi_{i\sigma} + \sum_{\rho=\uparrow,\downarrow} a_{\sigma,\rho} \psi_{a\rho}) \exp(ik_F x) + \sum_{\rho=\uparrow,\downarrow} b_{\sigma,\rho} \psi_{b\rho} \exp(-ik_F x) \right] \quad (25)$$

with  ${}^T\psi_{i\uparrow} = {}^T\psi_{b\uparrow} = (1, 0, 0, 0)$ ,  ${}^T\psi_{i\downarrow} = {}^T\psi_{b\downarrow} = (0, 1, 0, 0)$ ,  ${}^T\psi_{a\uparrow} = (0, 0, 1, 0)$ , and  ${}^T\psi_{a\downarrow} = (0, 0, 0, 1)$ . The corresponding  $\Psi_S(x)$  is given by Eq. (17). The coefficients  $a_{\sigma,\rho}$  and  $b_{\sigma,\rho}$  are determined by postulating the boundary condition  $\Psi_N(0) = \Psi_S(0)$ , and  $\hbar\hat{v}_{Sx}\Psi_S(0) - \hbar\hat{v}_{Nx}\Psi_N(0) = -2iU\hat{\tau}_3\Psi_S(0)$  with  $\hbar\hat{v}_{S(N)x} = \partial\hat{H}_{S(N)}/\partial k_x$ , and the diagonal matrix  $\hat{\tau}_3$  given by  $\hat{\tau}_3 = \text{diag}(1, 1, -1, -1)$ .

The resulting angle averaged charge conductance (tunneling conductance) is given by

$$\sigma_C \equiv \sigma_T = \left( \int_{-\pi/2}^{\pi/2} f_C(\theta) d\theta \right) / \left( \int_{-\pi/2}^{\pi/2} f_{NC}(\theta) d\theta \right). \quad (26)$$

We plot in Fig. 5 the charge conductance by changing the ratio of  $\Delta_s/\Delta_p$  in the presence of the splitting of the Fermi surface [40]. For  $\Delta_s < \Delta_p$ ,  $\sigma_T(eV)$  has a ZBCP due

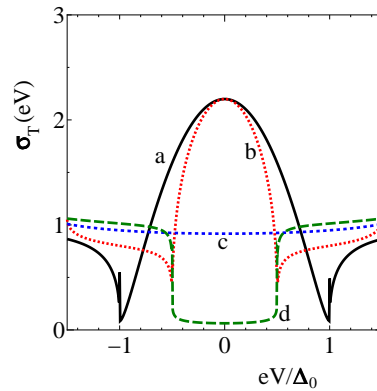


**Fig. 5** (Color online)  $\sigma_T$  for NCS superconductor with  $2m\lambda/k_F\hbar^2 = 0.1$  and  $Z = 5$ . a:  $\Delta_s = 0$ , b:  $\Delta_s = 0.5\Delta_p$ , c:  $\Delta_s = \Delta_p$  and d:  $\Delta_s = 1.5\Delta_p$ .

to the presence of the helical edge modes (curves *a* and *b* in Fig. 5). For  $\Delta_s = \Delta_p$ , due to the closing of the bulk energy gap, the resulting  $\sigma_T(eV)$  is almost constant. For  $\Delta_s > \Delta_p$ ,  $\sigma_T(eV)$  has a gap like structure similar to spin-singlet *s*-wave superconductor.

Next, we focus on the spin conductance. First we consider a pure  $(p_x \pm ip_y)$ -wave state. In Fig. 6, the angle resolved spin conductance is plotted as a function of injection angle  $\theta$  and bias voltage  $V$  with  $E = eV$ . Note here that the  $k_y$  is related to  $\theta$  as  $k_y = k_F \sin \theta$ . It is remarkable that the spin conductance has a non zero value although the NCS superconductor does not break time reversal symmetry. The quantity  $f_S(\theta)$  has a peak when the angle  $\theta$  or  $k_y$  corresponds to the Andreev bound state energy  $E$  in the energy dispersion. With this condition, the spin-dependent Andreev reflection occurs to result in a spin current. Besides this property, we can show that  $f_S(\theta) = -f_S(-\theta)$  is satisfied. By changing the sign of  $eV$ ,  $f_S(\theta)$  changes sign as seen in Fig. 6(a). Next, we look at the case where an *s*-wave component coexists. We calculate the spin conductance similar to that for the pure  $(p_x \pm ip_y)$ -wave case. For  $\Delta_s < \Delta_p$ , where helical edge modes exist,  $f_S(\theta)$  shows a sharp peak and  $f_S(\theta) = -f_S(-\theta)$  is satisfied [see Fig. 6(b)]. These features are similar to those of the pure  $(p_x \pm ip_y)$ -wave case. On the other hand, for  $\Delta_s > \Delta_p$ , where the helical edge modes are absent, sharp peaks of  $f_S(\theta)$  as shown in Fig. 6 are absent.

We have checked that there is negligible quantitative change, i.e., less than 0.5% change of the peak height, by taking the  $\lambda = 0$  limit compared to Fig. 6. In this limit, for the pure  $(p_x \pm ip_y)$ -wave state,  $f_S(\theta)$  is given simply as follows

$$\frac{-8RD^2 \sin 2\theta \sin 2\varphi \cos \theta}{|4(\sin^2 \theta - \sin^2 \varphi) + D[2 \cos 2\theta - (1 + R) \exp(-2i\varphi)]|^2}$$

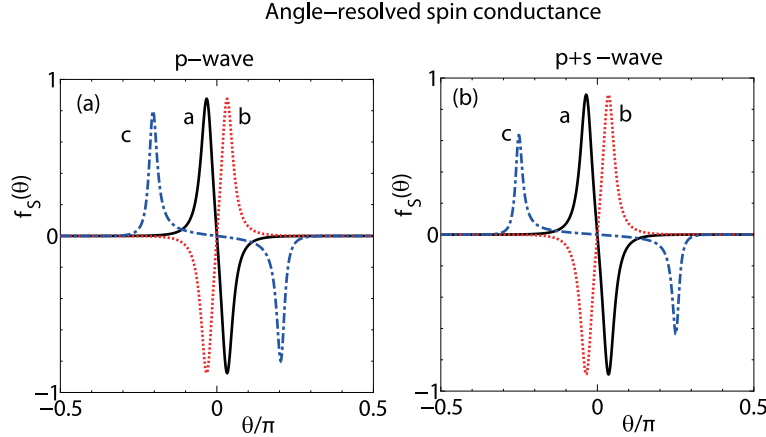


**Fig. 6** (Color online) Angle resolved spin conductance for  $Z = 5$ . a:  $eV = 0.1\Delta_p$ , b:  $eV = -0.1\Delta_p$  and c:  $eV = 0.6\Delta_p$  with  $\lambda k_F = 0.1\mu$ . (a) pure  $(p_x \pm ip_y)$ -wave case with  $\Delta_s = 0$ ; (b)  $\Delta_s = 0.3\Delta_p$ . [from Fig. 2 Phys. Rev. B **79**, 060505(R) (2009).]

for  $|E| < \Delta_p$  and  $f_S(\theta) = 0$  for  $|E| > \Delta_p$  with  $\sin \varphi = E/\Delta_p$ . The transparency of the interface  $D$  is given as before by  $4\cos^2\theta/(4\cos^2\theta + Z^2)$ , with the dimensionless constant  $Z = 2mU/\hbar^2k_F$ . The magnitude of  $f_S(\theta)$  is largely enhanced at  $E = \pm\Delta_p \sin\theta$  corresponding to the energy dispersion of the ABS. The origin of the nonzero  $f_S(\theta)$  even for  $\lambda = 0$  is due to spin-dependent Andreev bound states. We have checked that even if we take into account the spatial dependence of the  $(p_x \pm ip_y)$ -wave pair potential explicitly, the resulting  $f_S(\theta)$  does not qualitatively change [44].

Summarizing these features, we can conclude that the presence of the helical edge modes in NCS superconductors is the origin of the large angle resolved spin current through normal-metal/NCS superconductor junctions. However, the angle averaged normalized spin conductance becomes zero since  $f_S(\theta) = -f_S(-\theta)$  is satisfied.

Magnetic field offers an opportunity to observe the spin current in a more accessible way, where the time reversal (T) symmetry is broken by the shielding current at the interface. Here we consider the angle averaged normalized spin conductance  $\sigma_S$  and charge conductance  $\sigma_C$  as a function of magnetic field. The spin conductance is given by [47]

$$\sigma_S = \left( \int_{-\pi/2}^{\pi/2} f_S(\theta) d\theta \right) / \left( \int_{-\pi/2}^{\pi/2} f_{NC}(\theta) d\theta \right), \quad (27)$$

where  $f_{NC}(\theta)$  denotes the angle resolved charge conductance in the normal state with  $\Delta_p = \Delta_s = 0$ . We consider a magnetic field  $H$  applied perpendicular to the two-dimensional plane, which induces a shielding current along the normal-metal/NCS superconductor interface. When the penetration depth of the NCS superconductor is much longer than the coherence length, the vector potential can be approximated as described in section 2.2. As in the case of a chiral  $p$ -wave superconductor, the applied magnetic field shifts the quasiparticle energy  $E$  to  $E + H\Delta_p \sin\theta/H_0$ . For typical values of  $\xi \sim 10$  nm,  $\lambda_m \sim 100$  nm, the magnitude of  $H_0$  is of the order of 0.2 Tesla. The order of magnitude of the Doppler shift is given by  $H\Delta_p/H_0$ . Since the Zeeman energy is given by  $\mu_B H$ , the energy shift due to the Doppler effect is by a factor  $k_F \lambda_m$  larger than that due to the Zeeman effect. Thus, we can neglect the Zeeman effect in the present analysis. This is in sharp contrast to quantum spin Hall systems where the Zeeman effect is the main effect of a magnetic field, which opens a gap in the helical edge modes and modulates the transport properties [48]. The enhanced spin current due to Doppler shifts is specific to the superconducting state, and is not realized in quantum spin Hall systems.

### 2.3.3 Topological aspects

We now focus on the topological aspect of non-centrosymmetric superconductors. Recently, the concept of the quantum Hall system has been generalized to time-reversal (T) symmetric systems, i.e., quantum spin Hall systems [49–51]. A quan-

tum spin Hall system could be regarded as two copies of a quantum Hall system, for up and down spins, that are characterized by opposite chiralities. In the generic case, however, a mixture of up and down spins occurs due to spin-orbit interaction, which necessitates a new topological number to characterize a quantum spin Hall system [49, 51]. In quantum spin Hall systems, there exist helical edge modes, i.e., time-reversed partners of right- and left-going one-dimensional modes. This has been experimentally demonstrated for the quantum well of the HgTe system by measurements of the charge conductance [48].

As shown in Fig. 6, to discuss the topological nature of the helical edge modes, it is sufficient to consider the pure  $(p_x \pm ip_y)$ -wave state. Here, we give an argument from the viewpoint of the  $Z_2$  (topological) class [49], why the superconducting state with  $\Delta_p > \Delta_s$  has an Andreev bound state. We commence with a pure  $(p_x \pm ip_y)$ -wave state without spin-orbit interaction, i.e.  $\lambda = 0$ . The spin Chern number [51] for the corresponding Bogoliubov-de Gennes Hamiltonian is 2. Turning on  $\lambda$  adiabatically leaves the time reversal  $T$ -symmetry intact and keeps the gap open. Upon this adiabatic change of  $\lambda$ , the number of the helical edge mode pairs does not change. The reason is that this number is a topological number and consequently can only change by integer values. We now increase the magnitude of  $\Delta_s$  from zero. As far as  $\Delta_p > \Delta_s$  is satisfied, the number of helical edge modes does not change. However, if  $\Delta_s$  exceeds  $\Delta_p$ , the helical mode disappears. In this regime, the topological nature of the superconducting state belongs to a pure  $s$ -wave state with  $\lambda = 0$ . It is remarkable that just at  $\Delta_s = \Delta_p$  one of the two energy gaps for quasiparticles in the bulk closes. At precisely this point a quantum phase transition occurs.

In the following, we discuss the pure  $(p_x \pm ip_y)$ -wave case in more detail. In Fig. 7, the spin conductance  $\sigma_S$  and charge conductance  $\sigma_C$  normalized by the charge conductance in the normal state are plotted. It should be noted that  $\sigma_S$  becomes

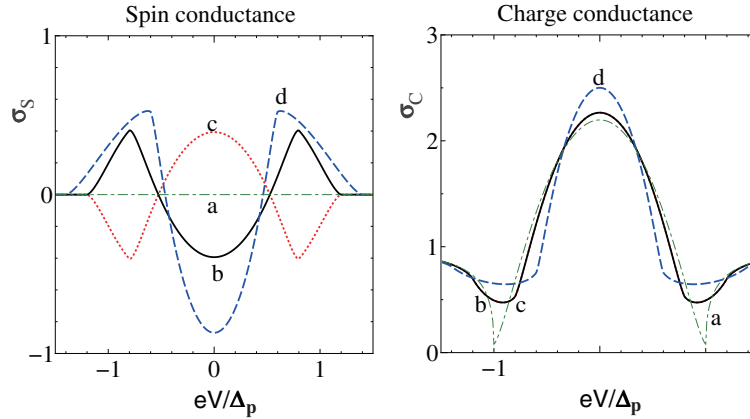


**Fig. 7** (Color online) Angle averaged spin conductance and charge conductance as a function of  $eV$  with bias voltage  $V$  with  $\lambda k_F = 0.1\mu$ . a:  $H = 0$ , b:  $H = -0.2H_0$ , c:  $H = 0.2H_0$ , and d:  $H = -0.4H_0$ . Curves  $b$  and  $c$  of the right panel are identical. [from Fig. 2 Phys. Rev. B **79**, 060505(R) (2009).]

nonzero in the presence of a magnetic field  $H$  (see curves  $b$ ,  $c$  and  $d$ ), since  $f_S(\theta)$  is no more an odd function of  $\theta$  due to the imbalance of the helical edge modes. For  $\lambda = 0$ , the corresponding helical edge modes are given by  $E = \Delta_p(1 - H/H_0) \sin \theta$  and  $E = -\Delta_p(1 + H/H_0) \sin \theta$ . As seen from the curves  $b$  and  $c$ , the sign of  $\sigma_S$  is reversed when changing the direction of the applied magnetic field. On the other hand, the corresponding charge conductance has different features. For  $H = 0$ , the resulting line shape of  $\sigma_C$  is the same as that for a chiral  $p$ -wave superconductor (see curve  $a$  of right panel) [42, 43, 45]. As seen from curves  $b$  and  $c$  in the right panel,  $\sigma_C$  does not change with the direction of the magnetic field  $H$ .

In summary, we have clarified the charge and spin transport properties of non-centrosymmetric superconductors from the viewpoint of topology and Andreev bound state. We have found an incident angle dependent spin polarized current flowing through the interface. When a weak magnetic field is applied, even the angle-integrated current is largely spin polarized. In analogy to quantum spin Hall systems, the Andreev bound states in non-centrosymmetric superconductors corresponds to helical edge modes. Andreev reflection via helical edge modes produces the enhanced spin current specific to non-centrosymmetric superconductors.

### 3 Quasiclassical Theory of Superconductivity for Non-Centrosymmetric Superconductors

#### 3.1 Quasiparticle Propagator

Electronic quasiparticles in normal Landau Fermi liquids are restricted in phase space to a region that comprises only a small part of the entire electronic phase space [52, 53]. It consists of a narrow (compared to the Fermi momentum  $\mathbf{p}_F$ ) shell around the Fermi surface, and a small (compared to the Fermi energy  $E_F$ ) region around the chemical potential. Quasiparticles are characterized by their spin and charge, and their group velocity is the Fermi velocity,  $\mathbf{v}_F(\mathbf{p}_F)$ . Quasiclassical theory is the appropriate framework to describe such a system. It consists of a *systematic* classification of all interaction processes according to their relevance, i.e. their smallness with respect to an expansion parameter SMALL [54–58]. This expansion parameter assumes the existence of a well defined scale separation between a *low-energy scale* and a *high-energy scale*.

Superconducting phenomena are governed by the low-energy scale. That means that the energy scales determined by the energy gap  $\Delta$  and the transition temperature  $T_c$  are small. In contrast the energy scales determined by the Fermi energy  $E_F$  or the Coulomb repulsion  $U_C$  are large energies. Disorder can be described within quasiclassical approximation as long as the energy associated with the scattering rate,  $\hbar/\tau$ , is classified as a small energy. A systematic classification shows that a consistent treatment of disorder requires the  $t$ -matrix approximation. Localization effects due to disorder are beyond the leading order precision of quasiclassical the-

ory. Associated with the energy scales are small and large length scales. For example the superconducting coherence length  $\xi_0 = \hbar v_F / 2\pi k_B T_c$ , and the elastic mean free path  $\ell = v_F \tau$  are large compared to the lattice constant  $a$  and the Fermi wave length  $\lambda_F = \hbar / p_F$ .

This separation in energy and length scales is associated with a low-energy region in phase space, that includes low quasiparticle energies  $\sim \Delta, k_B T$ , and a momentum shell around the quasiparticle Fermi momentum  $\mathbf{p}_F$  of extend  $\delta p \sim \Delta / |\mathbf{v}_F(\mathbf{p}_F)|$ . The phase space volume of this low-energy region, divided by the entire phase space volume, is employed for a systematic diagrammatic expansion of a Dyson series within a path-ordered Green's function technique (e.g. Matsubara technique for the Matsubara path, Keldysh-Nambu-Gor'kov technique for the Schwinger-Keldysh path). Within the framework of Green's function technique, all diagrams in a Feynman diagrammatic expansion can be classified according to their order in this expansion parameter, which is denoted as SMALL. The leading order theory in this expansion parameter is called the "Quasiclassical Theory of Metals and Superconductors" [54, 59, 60].

The possibility to define a quasiparticle Fermi surface around which all quasiparticle excitations reside is a requirement for the quasiclassical theory to work. Its presence ensures that the Pauli principle is still effective in placing stringent kinetic restrictions on the possible scattering events. It is essential to note that such a definition need not be sharp, i.e. the theory is not restricted to normal Fermi liquids with a jump in the momentum distribution at zero temperature. Thus, the theory includes superconducting phenomena as well as strong coupling metals. It is convenient to introduce a local coordinate system at each momentum point of the Fermi surface  $\mathbf{p}_F$ , with a variation along the surface normal, i.e. in direction of the Fermi velocity  $\mathbf{v}_F(\mathbf{p}_F)$ , that is determined by a variable  $\xi_{\mathbf{p}}$  (this variable is zero at the Fermi momentum), and a tangential variation along the Fermi surface at constant  $\xi_{\mathbf{p}}$ . A consistent approximation requires to consider the Fermi velocity constant across the low-energy momentum shell, and thus the local coordinate system stays an orthogonal system as long as  $\xi_{\mathbf{p}}$  varies within this momentum shell, and furthermore,  $\xi_{\mathbf{p}}$  stays small within this momentum shell. The coordinate  $\xi_{\mathbf{p}}$  around each Fermi surface point  $\mathbf{p}_F$  varies then approximately as  $\xi_{\mathbf{p}} \approx \mathbf{v}_F(\mathbf{p} - \mathbf{p}_F)$ .

The quasiclassical theory is obtained by defining quasiparticle propagators for the low-energy regions of the phase space, and in combining all diagrams involving Green's functions with their variables residing in the high-energy regions into new effective *high-energy interaction vertices*. This process of integrating out high-energy degrees of freedom is highly non-trivial and must be solved by microscopic theories. In the spirit of Fermi liquid theory it is, however, possible to regard all high-energy interaction vertices as phenomenological parameters of the theory. In quasiclassical approximation they do not depend on any low-energy variables as temperature or superconducting gap, and they do not vary as function of  $\xi_{\mathbf{p}}$  as long as  $\xi_{\mathbf{p}}$  stays within the momentum shell that harbors the quasiparticle excitations. However they do depend in general on the position of the Fermi momentum on the Fermi surface.



In addition to introducing new effective interaction vertices the above procedure also introduces a quasiparticle renormalization factor  $a^2(\mathbf{p}) \sim 1/Z(\mathbf{p})$ , that is due to the self energies of the low-energy quasiparticles moving in the background of the high energy electrons. This renormalization leads to a modification of the quasiparticle Fermi velocity compared to the bare Fermi velocity of the system, and to a deformation of the quasiparticle Fermi surface compared to the bare Fermi surface. It also determines quasiparticle weight as the residua of the quasiparticle poles in the complex energy plane.

One has to keep these remarks in consideration when including additional interaction, like spin-orbit interaction or exchange interaction, in a quasiclassical theory. First, it is important to decide if this interaction is going to be treated among the low-energy terms or among the high-energy terms. Depending on that one obtains two different quasiclassical theories, that cannot in general adiabatically be connected with each other. Going from one limit to the other includes the un-dressing of all effective interaction vertices and of the quasiparticles, and re-dressing with new types of effective interaction vertices and self energies. Importantly, this dressing leads to strongly spin dependent effective interactions and quasiparticle renormalizations in one limit, and to leading order spin-symmetric interactions and quasiparticle renormalizations in the other limit. The former case, when spin-dependent interactions are included in the high-energy scale, leads to a complete reorganization of the Fermi surface geometry, with in general new spin-dependent quasiparticle energy bands. In this case, it is not sensible anymore to keep the spin as a good quantum number, but it is necessary to deal directly with the representation that diagonalizes the energy bands including the spin-dependent interaction. In the case of a strong exchange energy this leads to exchange split energy bands, and in the case of strong spin-orbit interaction this leads to helicity bands.

The basic quantities in the theory are the quasiparticle Fermi surface, the quasiparticle velocity, and quasiparticle interactions. Here we give a short sketch of how they enter the theory. The bare propagator (without inclusion of exchange interaction or spin-orbit coupling) in the quasiparticle region of the phase space has the general structure

$$G_{\alpha\beta}^{(0)}(\mathbf{p}, \varepsilon) = \frac{\delta_{\alpha\beta}}{\varepsilon - \xi^{(0)}(\mathbf{p})} \quad (28)$$

where  $\xi^{(0)}(\mathbf{p})$  is the bare energy dispersion of the energy band (measured from the electrochemical potential of the electrons). It does not include electron-electron interaction effects yet, and thus determines a *bare* Fermi surface that does not coincide with the quasiparticle Fermi surface defined below. The quantum number  $\alpha$  labels the spin. The leading order self energy is solely due to coupling of low-energy electrons (superscript L) to high-energy electrons (superscript H), and consequently the corresponding self energy,  $\Sigma^{(H)}$ , must be classified as a pure high-energy quantity. In general, when either exchange interaction or spin-orbit coupling are large energy scales, this self energy contribution will be spin-dependent (and will ultimately lead to new, spin-split energy bands as explained below). The self energy  $\Sigma^{(H)}$  is, however, slowly varying in energy on the low-energy scale and thus can be expanded

around the chemical potential,

$$\Sigma_{\alpha\beta}^{(H)}(\mathbf{p}, \varepsilon) = \Sigma_{\alpha\beta}^{(H)}(\mathbf{p}, 0) + \varepsilon \partial_{\varepsilon} \Sigma_{\alpha\beta}^{(H)}(\mathbf{p}, \varepsilon) \Big|_{\varepsilon=0} + \mathcal{O}(\varepsilon^2). \quad (29)$$

The second term can be combined with energy  $\varepsilon$  into a renormalization function

$$\varepsilon - \varepsilon \partial_{\varepsilon} \Sigma_{\alpha\beta}^{(H)}(\mathbf{p}, 0) = Z_{\alpha\beta}^{(H)}(\mathbf{p}) \varepsilon, \quad (30)$$

such that to leading order the Dyson equation for the low-energy propagator  $G_{\beta\gamma}^{(L)}$  reads

$$\left\{ Z_{\alpha\beta}^{(H)}(\mathbf{p}) \varepsilon - [\xi^{(0)}(\mathbf{p}) \delta_{\alpha\beta} + \Sigma_{\alpha\beta}^{(H)}(\mathbf{p}, 0) - \Sigma_{\alpha\beta}^{(L)}(\mathbf{p}, \varepsilon)] \right\} \otimes G_{\beta\gamma}^{(L)}(\mathbf{p}, \varepsilon) = \delta_{\alpha\gamma}, \quad (31)$$

where  $\Sigma^{(L)}$  includes all self energy terms of order SMALL. Here, and in the following, summation over repeated indices is implied. The  $\otimes$  sign accounts for possible spatial or temporal inhomogeneities, in which case it has the form of a convolution product in Wigner representation (see Ref. [54] for details). The equation holds in this form either in Matsubara or in Keldysh representation (in which case all quantities are  $2 \times 2$  matrices in Keldysh space [67]). Low-energy excitations reside in momentum regions differing considerably from that for the bare propagators Eq. (28).

The quantities  $Z_{\alpha\beta}^{(H)}(\mathbf{p})$  and  $\Sigma_{\alpha\beta}^{(H)}(\mathbf{p}, 0)$  can be defined such that they have real eigenvalues. The next step is to eliminate the high-energy renormalization factor  $Z_{\alpha\beta}^{(H)}(\mathbf{p})$  from the low-energy theory. This is done with the help of quasiparticle weight factors  $a_{\alpha\beta}(\mathbf{p})$ , that are the solution of

$$a_{\alpha\gamma}(\mathbf{p}) Z_{\gamma\gamma'}^{(H)}(\mathbf{p}) a_{\gamma\beta}(\mathbf{p}) = \delta_{\alpha\beta}. \quad (32)$$

They exist as long as  $Z_{\gamma\gamma'}^{(H)}$  has non-zero eigenvalues. Then we can define the *quasiparticle Green's function*  $G_{\alpha\beta}^{(QP)}$  as the solution of

$$a_{\alpha\gamma}(\mathbf{p}) G_{\gamma\gamma'}^{(QP)} a_{\gamma\beta}(\mathbf{p}) = G_{\alpha\beta}^{(L)}(\mathbf{p}, \varepsilon), \quad (33)$$

which exists under the condition that  $a_{\alpha\gamma}$  has non-zero eigenvalues (i.e. the quasiparticle weights are non-zero; otherwise the quasiparticle approximation breaks down). It fulfills the Dyson equation

$$[\varepsilon - \xi^{QP}(\mathbf{p}) - \Sigma^{QP}(\mathbf{p}, \varepsilon)]_{\alpha\beta} \otimes G_{\beta\gamma}^{(QP)}(\mathbf{p}, \varepsilon) = \delta_{\alpha\gamma} \quad (34)$$

with the quasiparticle dispersion

$$\xi_{\alpha\beta}^{(QP)}(\mathbf{p}) = a_{\alpha\gamma}(\mathbf{p}) \left( \xi^{(0)}(\mathbf{p}) \delta_{\gamma\gamma'} + \Sigma_{\gamma\gamma'}^{(H)}(\mathbf{p}, 0) \right) a_{\gamma\beta}(\mathbf{p}) \quad (35)$$

and the quasiparticle self energies

$$\Sigma_{\alpha\beta}^{(QP)}(\mathbf{p}, \varepsilon) = a_{\alpha\gamma}(\mathbf{p}) \Sigma_{\gamma\gamma'}^{(L)}(\mathbf{p}, \varepsilon) a_{\gamma'\beta}(\mathbf{p}). \quad (36)$$

The effective (renormalized by high-energy processes) interactions vertices for the low-energy propagators,  $G_{\alpha\beta}^{(L)}$ , which enter the diagrammatic expressions for the quasiparticle self energy, have the general structure  $V_{\beta_1 \dots \beta_n}(\varepsilon_1, \mathbf{p}_1; \dots; \varepsilon_n, \mathbf{p}_n)$ . In leading order the energy dependence of these vertices can be neglected near the chemical potential, i.e. the arguments can be restricted to the chemical potential. Furthermore, instead of working with  $G_{\alpha\beta}^{(L)}$  and  $V_{\beta_1 \dots \beta_n}$  the common and completely equivalent description in terms of the above defined quasiparticle propagators,  $G_{\alpha\beta}^{(QP)}$ , and renormalized quasiparticle interactions,  $V_{\beta_1 \dots \beta_n}^{(QP)}$ , given by

$$V_{\beta_1 \dots \beta_n}^{(QP)}(\mathbf{p}_1 \dots \mathbf{p}_n) = a_{\beta_1 \beta'_1}(\mathbf{p}_1) \dots a_{\beta_n \beta'_n}(\mathbf{p}_n) V_{\beta'_1 \dots \beta'_n}(0, \mathbf{p}_1; \dots; 0, \mathbf{p}_n) \quad (37)$$

can be used.

It is important to note that the quasiparticle self energies can be written down as functionals of the quasiparticle Green's functions only in leading order in the expansion in  $\text{SMALL}$ , which is the order relevant for the quasiclassical approximation. In this case, the quasiparticle weights have disappeared from the theory and cannot in principle be determined from low-energy processes that only involve quasiparticle dynamics. They must be obtained from a microscopic theory by considering high energy scattering processes, which is beyond the quasiclassical approximation.

It is obvious, that the appearance of the quasiparticle renormalization factors renders all self energies and interactions non-diagonal in spin unless spin-dependent interactions are small enough to be omitted from the high-energy quantities. From the above expressions one obtains the quasiparticle Fermi surfaces by diagonalizing the quasiparticle dispersion

$$U_{\mathbf{p}\lambda\alpha} \xi_{\alpha\beta}^{(QP)}(\mathbf{p}) = \xi_{\lambda}^{(QP)}(\mathbf{p}) U_{\mathbf{p}\lambda\beta} \quad (38)$$

with band index  $\lambda$ , and solving the equation

$$\xi_{\lambda}^{(QP)}(\mathbf{p}) = 0 \rightarrow \mathbf{p} = \mathbf{p}_F^{\lambda}. \quad (39)$$

The corresponding quasiparticle Fermi velocity is then given by

$$\mathbf{v}_F^{\lambda} = \frac{\partial}{\partial \mathbf{p}} \xi_{\lambda}^{(QP)}(\mathbf{p}) \Big|_{\mathbf{p}=\mathbf{p}_F^{\lambda}}. \quad (40)$$

In the band diagonal frame, the quasiparticle propagator is given by,

$$\left\{ [\varepsilon - \xi_{\lambda}^{QP}(\mathbf{p})] \delta_{\lambda\lambda_1} - \Sigma_{\lambda\lambda_1}^{QP}(\mathbf{p}, \varepsilon) \right\} \otimes G_{\lambda_1\lambda'}^{(QP)}(\mathbf{p}, \varepsilon) = \delta_{\lambda\lambda'}, \quad (41)$$

where the self energy (and all interactions in the self energy expressions) must be transformed accordingly, e.g.

$$\Sigma_{\lambda\lambda'}^{(QP)}(\mathbf{p}, \varepsilon) = U_{\mathbf{p}\lambda\alpha} \Sigma_{\alpha\beta}^{(QP)}(\mathbf{p}, \varepsilon) U_{\mathbf{p}\beta\lambda'}^*. \quad (42)$$

In the next section this procedure is carried out for the case of a strong spin-orbit interaction, e.g. appropriate for some non-centrosymmetric materials.

### 3.2 Spin-orbit interaction and Helicity representation

As discussed in the introductory chapter of this book, for treating a non-centrosymmetric material it is convenient to perform a canonical transformation from a spin basis with fermion annihilation operators  $a_{\mathbf{k}\alpha}$  for spin  $\alpha = \uparrow, \downarrow$  to the so-called helicity basis with fermion annihilation operators  $c_{\mathbf{k}\lambda}$  for helicity  $\lambda = \pm$ . This canonical transformation diagonalizes the kinetic part of the Hamiltonian,

$$\mathcal{H}_{kin} = \sum_{\mathbf{k}} \sum_{\alpha\beta=\uparrow,\downarrow} [\xi(\mathbf{k}) + \mathbf{g}(\mathbf{k}) \cdot \boldsymbol{\sigma}]_{\alpha\beta} a_{\mathbf{k}\alpha}^\dagger a_{\mathbf{k}\beta} = \sum_{\mathbf{k}} \sum_{\lambda=\pm} \xi_{\lambda}(\mathbf{k}) c_{\mathbf{k}\lambda}^\dagger c_{\mathbf{k}\lambda}. \quad (43)$$

Here,  $\xi(\mathbf{k})$  is the band dispersion relative to the chemical potential in the absence of spin-orbit interaction,  $\mathbf{g}(\mathbf{k})$  is the spin-orbit pseudovector, which is odd in momentum,  $\mathbf{g}(-\mathbf{k}) = -\mathbf{g}(\mathbf{k})$ , and  $\boldsymbol{\sigma}$  is the vector of Pauli matrices. The resulting helicity band dispersion is

$$\xi_{\pm}(\mathbf{k}) = \xi(\mathbf{k}) \pm |\mathbf{g}(\mathbf{k})|. \quad (44)$$

As is easily seen, spin-orbit interaction locks the orientation of the quasiparticle spin with respect to its momentum in each helicity band. The Hamiltonian, Eq. (43), is time reversal invariant, however lifts the spin degeneracy.

It is convenient to introduce polar and azimuthal angles for the vector  $\mathbf{g}$ , defined by  $\{g_x, g_y, g_z\} = |\mathbf{g}| \{\sin(\theta_g) \cos(\varphi_g), \sin(\theta_g) \sin(\varphi_g), \cos(\theta_g)\}$  (where  $0 \leq \theta_g \leq \pi$ ). In terms of those, the transformation from spin to helicity basis,  $U_{\mathbf{k}\lambda\alpha}$ , is defined by [36]

$$U_{\mathbf{k}\lambda\alpha} = \begin{pmatrix} \cos(\theta_g/2) & \sin(\theta_g/2)e^{-i\varphi_g} \\ -\sin(\theta_g/2)e^{i\varphi_g} & \cos(\theta_g/2) \end{pmatrix}, \quad c_{\mathbf{k}\lambda} = \sum_{\alpha} U_{\mathbf{k}\lambda\alpha} a_{\mathbf{k}\alpha}. \quad (45)$$

Obviously,  $\sum_{\alpha\beta} U_{\mathbf{k}\lambda\alpha} [\mathbf{g}(\mathbf{k}) \cdot \boldsymbol{\sigma}_{\alpha\beta}] U_{\mathbf{k}\lambda'\beta}^* = |\mathbf{g}(\mathbf{k})| \sigma_{\lambda\lambda'}^{(3)}$ .

For the superconducting state the Nambu-Gor'kov formalism is appropriate [66]. The Nambu spinor,  $\hat{A}_{\mathbf{k}} = (a_{\mathbf{k}\uparrow}, a_{\mathbf{k}\downarrow}, a_{-\mathbf{k}\uparrow}^\dagger, a_{-\mathbf{k}\downarrow}^\dagger)^T$  transforms under the above canonical transformation into the helical object  $\hat{C}_{\mathbf{k}} = (c_{\mathbf{k}+}, c_{\mathbf{k}-}, c_{-\mathbf{k}+}^\dagger, c_{-\mathbf{k}-}^\dagger)^T$ , where

$$\hat{C}_{\mathbf{k}} = \hat{U}_{\mathbf{k}} \hat{A}_{\mathbf{k}}, \quad \hat{U}_{\mathbf{k}} = \begin{pmatrix} U_{\mathbf{k}} & 0 \\ 0 & U_{-\mathbf{k}}^* \end{pmatrix}. \quad (46)$$

Correspondingly, one can construct  $4 \times 4$  retarded Green's functions in spin basis,

$$\hat{G}_{\mathbf{k}_1\mathbf{k}_2}^{(s)}(t_1, t_2) = -i\theta(t_1 - t_2) \langle \{ \hat{A}_{\mathbf{k}_1}(t_1), \hat{A}_{\mathbf{k}_2}^\dagger(t_2) \} \rangle_{\mathcal{H}}, \quad (47)$$

and in helicity basis,

$$\hat{G}_{\mathbf{k}_1\mathbf{k}_2}(t_1, t_2) = -i\theta(t_1 - t_2) \langle \{ \hat{C}_{\mathbf{k}_1}(t_1), \hat{C}_{\mathbf{k}_2}^\dagger(t_2) \} \rangle_{\mathcal{H}} = \hat{U}_{\mathbf{k}_1} \hat{G}_{\mathbf{k}_1\mathbf{k}_2}^{(s)}(t_1, t_2) \hat{U}_{\mathbf{k}_2}^\dagger, \quad (48)$$

where  $\hat{A}(t)$  and  $\hat{C}(t)$  are Heisenberg operators, the braces denote an anticommutator,  $\langle \dots \rangle_{\mathcal{H}}$  is a grand canonical average, and  $\theta$  is the usual Heaviside step function. Analogously, advanced, Keldysh, and Matsubara propagators can be defined in helicity representation. For dealing with superconducting phenomena it is often convenient to introduce Wigner coordinates,

$$\hat{G}(\mathbf{k}, \mathbf{R}, \varepsilon, t) = \int (d\mathbf{q})(d\tau) e^{i(\mathbf{q}\mathbf{R} + \varepsilon\tau)} \hat{G}_{\mathbf{k} + \frac{\mathbf{q}}{2}, \mathbf{k} - \frac{\mathbf{q}}{2}}(t + \frac{\tau}{2}, t - \frac{\tau}{2}). \quad (49)$$

From here, one can proceed along different lines. Either, the Dyson equation for the full Gor'kov Green's functions is solved, which is equivalent to the Bogoliubov-de Gennes description in wave function techniques. Or, the quasiclassical approximation is employed, that is equivalent to the Andreev approximation in wave function language. In the following section we will adopt the second line.

### 3.3 Quasiclassical Propagator

In the following, the quasiclassical theory of superconductivity [54, 59–65] will be employed to calculate electronic transport properties across interfaces with non-centrosymmetric superconductors. This method is based on the observation that, in most situations, the superconducting state varies on the length scale of the superconducting coherence length  $\xi_0 = \hbar v_F / 2\pi k_B T_c$ . The appropriate many-body Green's function for describing the superconducting state has been introduced by Gor'kov [66], and the Gor'kov Green's function can then be decomposed in a fast oscillating component, varying on the scale of  $1/k_F$ , and an envelop function varying on the scale of  $\xi_0$ . The quasiclassical approximation consists of integrating out the fast oscillating component for each quasiparticle band separately:

$$\check{g}(\mathbf{p}_F^\lambda, \mathbf{R}, \varepsilon, t) = \int d\xi_{\mathbf{p}}^\lambda \hat{v}_3 \check{G}^{(\text{QP})}(\mathbf{p}, \mathbf{R}, \varepsilon, t) \quad (50)$$

where a “check” denotes a matrix in Keldysh-Nambu-Gor'kov space, [67] a “hat” denotes a matrix in Nambu-Gor'kov particle-hole space,  $\xi_{\mathbf{p}}^\lambda = v_F^\lambda(\mathbf{p} - \mathbf{p}_F^\lambda)$ , and  $\hat{v}_3$  is the third Pauli matrix in particle-hole space.

The quasiclassical Green's function obeys the transport equation [59, 60]

$$i\hbar v_F \cdot \nabla_{\mathbf{R}} \check{g} + [\varepsilon \hat{v}_3 - \check{\Delta} - \check{h}, \check{g}]_{\circ} = \check{0}. \quad (51)$$

Here,  $\varepsilon$  is the quasiparticle energy,  $\check{\Delta}$  is the superconducting order parameter and  $\check{h}$  contains all other self-energies and external perturbations, related to external fields, impurities etc. The notation  $\circ$  combines a time convolution with matrix multiplica-

tion, and  $[\bullet, \bullet]_{\circ}$  denotes the commutator with respect to the  $\circ$ -product. Equation (51) must be supplemented by a normalization condition that must be obtained from an explicite calculations in the normal state [59, 68],

$$\check{g} \circ \check{g} = -\check{1}\pi^2. \quad (52)$$

From the knowledge of  $\check{g}$  one can calculate measurable quantities, e.g. the current density is related to the Keldysh component of the Green's function via

$$\mathbf{j}(\mathbf{R}, t) = qN_F \int \frac{d\varepsilon}{8\pi i} \text{Tr} \langle \mathbf{v}_F \hat{\tau}_3 \hat{g}^K(\mathbf{p}_F^\lambda, \mathbf{R}, \varepsilon, t) \rangle, \quad (53)$$

where  $q = -|e|$  is the electron charge, and  $\langle \dots \rangle$  denotes a Fermi surface average, which is defined by

$$\langle \dots \rangle = \frac{1}{N_F} \sum_{\lambda} \int \frac{d^3 p_F^\lambda}{(2\pi\hbar)^3 |\mathbf{v}_F^\lambda|} \dots \quad N_F = \sum_{\lambda} \int \frac{d^3 p_F^\lambda}{(2\pi\hbar)^3 |\mathbf{v}_F^\lambda|}, \quad (54)$$

and Tr denotes a trace over the Nambu-Gor'kov matrix.

### 3.3.1 Case of weak spin-orbit splitting

In the case of weak spin-orbit splitting the quasiclassical propagator can be obtained in either spin or helicity representation. It is possible then to define a common Fermi surface  $\mathbf{p}_F$  for both spin bands or, equivalently, both helicity bands. This case applies when  $|\mathbf{g}(\mathbf{p}_F)| \ll E_F$  for any Fermi momentum  $\mathbf{p}_F$ , where  $E_F$  is the Fermi energy (in addition to the condition that the superconducting energy scales ( $k_B T_c$  and the gap  $\Delta$  are much smaller than  $E_F$ ). Under these circumstances quasiparticles with different helicity but with the same  $\hat{\mathbf{k}} \equiv \mathbf{k}/|\mathbf{k}|$  propagate coherently along a common classical trajectory over distances much longer than the Fermi wavelength. The transport equation is the usual Eilenberger equation modified by a spin-orbit interaction term [54, 69]

$$i\hbar \mathbf{v}_F \cdot \nabla_{\mathbf{R}} \check{g} + [\varepsilon \hat{\tau}_3 - \check{\Delta} - \check{v}_{SO}, \check{g}]_{\circ} = \check{0} \quad (55)$$

with normalization  $\hat{g} \circ \hat{g} = -\pi^2 \hat{1}$ . Here, in helicity basis  $\hat{v}_{SO} = |\mathbf{g}_{\mathbf{k}_F}| \sigma^{(3)}$ , and in spin basis  $\hat{v}_{SO} = \mathbf{g}_{\mathbf{k}_F} \cdot \hat{\sigma} \hat{\tau}_3$ , with

$$\hat{\sigma} = \begin{pmatrix} \sigma & 0 \\ 0 & \sigma^* \end{pmatrix} = \begin{pmatrix} \sigma & 0 \\ 0 & -\sigma^{(2)} \sigma \sigma^{(2)} \end{pmatrix}. \quad (56)$$

The velocity renormalization of order  $|\mathbf{g}|/E_F \ll 1$  can safely be neglected. The quasiparticle trajectories are doubly degenerate in either spin or helicity space, and coherent mixing between spin states or between helicity states can take place.

### 3.3.2 Case of strong spin-orbit splitting

In the case of strong spin-orbit splitting the only possible representation for quasiclassical theory is the helicity representation. In this case, the spin-orbit interaction does not appear anymore as a source term in the transport equations, however explicitly as the presence of well defined helicity bands. The transport equation takes the form

$$i\hbar\mathbf{v}_F^\lambda \cdot \nabla_{\mathbf{R}}\check{g} + [\varepsilon\hat{t}_3 - \check{\Delta}^\lambda, \check{g}]_o = \check{0} \quad (57)$$

with normalization condition  $\hat{g} \circ \hat{g} = -\pi^2 \hat{1}$ . Here, the velocity is strongly renormalized due to spin-orbit interaction. The quasiparticle trajectories are different for different helicity, and no coherence exists between the different helicity states. The matrix dimension can be reduced by a factor 2 compared to the case of weak spin-orbit splitting, and instead the number of Fermi surface sheets is increased by a factor of 2. If measurements are made that are spin-selective, the corresponding vector of Pauli spin matrices must be transformed according to

$$\sigma_{\lambda\lambda'} = (U_{\mathbf{k}}\sigma U_{\mathbf{k}}^\dagger)_{\lambda\lambda'} = U_{\mathbf{k}\lambda\alpha}\sigma_{\alpha\beta}U_{\mathbf{k}\lambda'\beta}^* \quad (58)$$

### 3.4 Riccati parameterization

One of the main obstacles of quasiclassical theory has been the non-linearity that is introduced by the normalization condition. A powerful way to deal with this problem is the choice of a parameter representation that ensures the normalization condition by definition. In this representation, the Keldysh quasiclassical Green's function is determined by six parameters in particle-hole space,  $\gamma^{R,A}, \tilde{\gamma}^{R,A}, x^K, \tilde{x}^K$ , of which  $\gamma^{R,A}, \tilde{\gamma}^{R,A}$  are the coherence functions, describing the coherence between particle-like and hole-like states, whereas  $x^K, \tilde{x}^K$  are distribution functions, describing the occupation of quasiparticle states [20, 70]. The coherence functions are a generalization of the so-called Riccati amplitudes [70–74] to non-equilibrium situations. All six parameters are matrix functions with the dimension determined by the degeneracy of the quasiparticle trajectories, and depend on Fermi momentum, position, energy, and time. The parameterization is simplified by the fact that, due to symmetry relations, only two functions of the six are independent. The particle-hole symmetry is expressed by the operation  $\tilde{X}$  which is defined for any function  $X$  of the phase space variables by

$$\tilde{Q}(\mathbf{p}_F, \mathbf{R}, z, t) = Q(-\mathbf{p}_F, \mathbf{R}, -z^*, t)^* \quad (59)$$

Here,  $z = \varepsilon$  is real for the Keldysh components and  $z$  is situated in the upper (lower) complex energy half plane for retarded (advanced) quantities. Furthermore, the symmetry relations

$$\gamma^A = (\tilde{\gamma}^R)^\dagger, \quad \tilde{\gamma}^A = (\gamma^R)^\dagger, \quad x^K = (\tilde{x}^K)^\dagger \quad (60)$$

hold. As a consequence, it suffices to determine fully the parameters  $\gamma^{\mathbf{R}}$  and  $x^{\mathbf{K}}$ .

The quasiclassical Green's function is related to these amplitudes in the following way [here the upper (lower) sign corresponds to retarded (advanced)]:

$$\hat{g}^{\mathbf{R},\mathbf{A}} = \mp i\pi \begin{pmatrix} (1 - \gamma \circ \tilde{\gamma})^{-1} \circ (1 + \gamma \circ \tilde{\gamma}) & 2(1 - \gamma \circ \tilde{\gamma})^{-1} \circ \gamma \\ -2(1 - \tilde{\gamma} \circ \gamma)^{-1} \circ \tilde{\gamma} & -(1 - \tilde{\gamma} \circ \gamma)^{-1} \circ (1 + \tilde{\gamma} \circ \gamma) \end{pmatrix}^{\mathbf{R},\mathbf{A}}, \quad (61)$$

which can be written in more compact form as [82]

$$\hat{g}^{\mathbf{R},\mathbf{A}} = \mp 2\pi i \begin{pmatrix} \mathcal{G} & \mathcal{F} \\ -\tilde{\mathcal{F}} & -\tilde{\mathcal{G}} \end{pmatrix}^{\mathbf{R},\mathbf{A}} \pm i\pi \hat{t}_3, \quad (62)$$

with the abbreviations  $\mathcal{G} = (1 - \gamma \circ \tilde{\gamma})^{-1}$  and  $\mathcal{F} = \mathcal{G} \circ \gamma$ . For the Keldysh component one can write [82]

$$\hat{g}^{\mathbf{K}} = -2\pi i \begin{pmatrix} \mathcal{G} & \mathcal{F} \\ -\tilde{\mathcal{F}} & -\tilde{\mathcal{G}} \end{pmatrix}^{\mathbf{R}} \circ \begin{pmatrix} x^{\mathbf{K}} & 0 \\ 0 & \tilde{x}^{\mathbf{K}} \end{pmatrix} \circ \begin{pmatrix} \mathcal{G} & \mathcal{F} \\ -\tilde{\mathcal{F}} & -\tilde{\mathcal{G}} \end{pmatrix}^{\mathbf{A}}. \quad (63)$$

Here, the  $\circ$ -symbol includes a time convolution as well as matrix multiplication; the inversion is defined with respect to the  $\circ$ -operation [82].

From the transport equation for the quasiclassical Green's functions one obtains a set of matrix equations of motion for the six parameters above [20, 70]. For the coherence amplitudes this leads to Riccati differential equations [72], hence the name Riccati parameterization.

### 3.5 Transport equations

The central equations that govern the transport phenomena have been derived in Ref. [20, 70]. The transport equation for the coherence functions  $\gamma(\mathbf{p}_F, \mathbf{R}, \varepsilon, t)$  are given by

$$(i\hbar \mathbf{v}_F \cdot \nabla_{\mathbf{R}} + 2\varepsilon)\gamma^{\mathbf{R},\mathbf{A}} = [\gamma \circ \tilde{\Delta} \circ \gamma + \Sigma \circ \gamma - \gamma \circ \tilde{\Sigma} - \Delta]^{\mathbf{R},\mathbf{A}}. \quad (64)$$

For the distribution functions  $x(\mathbf{p}_F, \mathbf{R}, \varepsilon, t)$  the transport equations read

$$\begin{aligned} (i\hbar \mathbf{v}_F \cdot \nabla_{\mathbf{R}} + i\hbar \partial_t)x^{\mathbf{K}} - [\gamma \circ \tilde{\Delta} + \Sigma]^{\mathbf{R}} \circ x^{\mathbf{K}} - x^{\mathbf{K}} \circ [\Delta \circ \tilde{\gamma} - \Sigma]^{\mathbf{A}} \\ = -\gamma^{\mathbf{R}} \circ \tilde{\Sigma}^{\mathbf{K}} \circ \tilde{\gamma}^{\mathbf{A}} + \Delta^{\mathbf{K}} \circ \tilde{\gamma}^{\mathbf{A}} + \gamma^{\mathbf{R}} \circ \tilde{\Delta}^{\mathbf{K}} - \Sigma^{\mathbf{K}}. \end{aligned} \quad (65)$$

The equations for the remaining components are obtained by the symmetry relation Eq. (59).



### 3.6 Boundary conditions

The transport equations must be complemented with boundary conditions for the coherence amplitudes and distribution functions at interfaces and surfaces [75, 76]. For spin-active scattering such conditions were obtained in Ref. [77]. Explicit formulations in terms of special parameterizations were given in Refs. [20, 78–81]. Further developments include strongly spin-polarized systems [82–86], diffusive interface scattering [87] or multi-band systems [88]. We adopt the notation [20] that incoming amplitudes are denoted by small case letters and outgoing ones by capital case letters, see Fig. 8. Note that the velocity direction of trajectories is opposite for holelike and particlelike amplitudes as well as advanced and retarded ones. The boundary conditions express outgoing amplitudes as a function of incoming ones and as a function of the parameters of the normal-state scattering matrix.

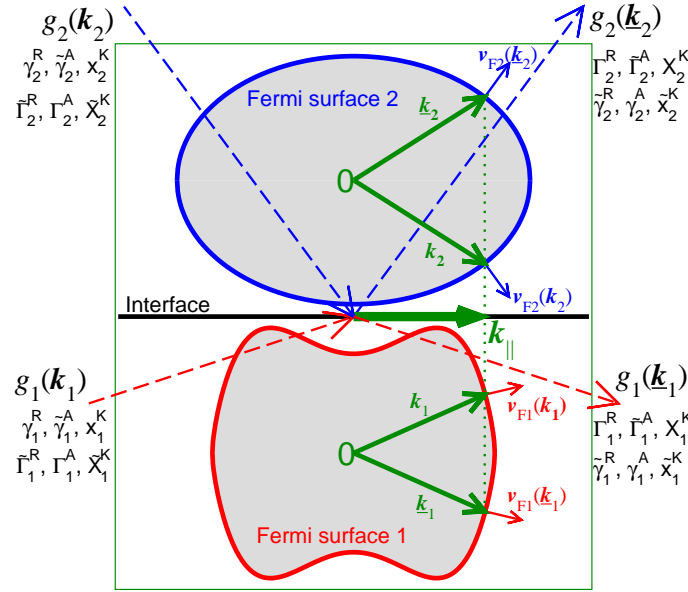


**Fig. 8** Notation for the coherence amplitudes and distribution functions at an interface. Indices 1 and 2 refer to the sides of the interface. The arrows for the Fermi momenta are for particle like excitations. The Fermi velocity directions are given by the directions perpendicular to the Fermi surface at the corresponding Fermi momentum. Quasiparticles move along the Fermi velocity directions (dashed lines). The components of the Fermi momenta parallel to the surface are conserved (indicated by the thin dotted line). For each trajectory, small case letters denote coherence functions and distribution functions with initial conditions from the bulk, and capital case letters denote functions with initial conditions at the interface. The interface boundary conditions must express all capital case quantities in terms of the small case quantities. Here, the simplest case, that involves only one Fermi surface sheet on either side ('two-trajectory scattering'), is shown. After Ref. [20].

### 3.6.1 Coherence amplitudes

The boundary conditions for the coherence amplitudes are formulated in terms of the solution of the equation [82]

$$[\gamma'_{kk'}]^R = \sum_p S_{kp}^R \circ \gamma_p^R \circ \tilde{S}_{pk'}^R \quad (66)$$

$$[\Gamma_{k \leftarrow k'}]^R = [\gamma'_{kk'}]^R + \sum_{k_1 \neq k} \Gamma_{k \leftarrow k_1} \circ \tilde{\gamma}_{k_1} \circ \gamma'_{k_1 k'}]^R, \quad (67)$$

(the trajectory index  $p$  runs over all incoming trajectories) for  $[\Gamma_{k \leftarrow k'}]^R$ , where the trajectory indices  $k, k', k_1$  run over outgoing trajectories involved in the interface scattering process, and the scattering matrix parameters enter only via the “elementary scattering event”  $[\gamma'_{kk'}]^R, A$ . The quasiclassical coherence amplitude is given by the forward scattering contribution of  $[\Gamma_{k \leftarrow k'}]^R$ ,

$$\Gamma_k^R = \Gamma_{k \leftarrow k}^R. \quad (68)$$

Analogous equations [82] hold for the advanced and particle-hole conjugated components,  $[\tilde{\Gamma}_{p \leftarrow p'}]^R$ ,  $[\Gamma_{p' \rightarrow p}]^A$ , and  $[\tilde{\Gamma}_{k' \rightarrow k}]^A$ .

### 3.6.2 Distribution functions

For the Keldysh component not only the forward scattering contribution of  $[\Gamma_{k \leftarrow k'}]^R$  is required, but also the off-scattering part

$$[\bar{\Gamma}_{k \leftarrow k'}]^R = [\Gamma_{k \leftarrow k'} - \Gamma_k \delta_{kk'}]^R. \quad (69)$$

The boundary conditions for the distribution functions read [82]

$$[x'_{kk'}]^K = \sum_p S_{kp}^R \circ x_p^K \circ S_{pk'}^A. \quad (70)$$

$$\begin{aligned} X_k^K &= \sum_{k_1, k_2} [\delta_{kk_1} + \bar{\Gamma}_{k \leftarrow k_1} \circ \tilde{\gamma}_{k_1}]^R \circ [x'_{k_1 k_2}]^K \circ [\delta_{k_2 k} + \gamma_{k_2} \circ \bar{\Gamma}_{k_2 \rightarrow k}]^A \\ &\quad - \sum_{k_1} [\bar{\Gamma}_{k \leftarrow k_1}]^R \circ \tilde{x}_{k_1}^K \circ [\bar{\Gamma}_{k_1 \rightarrow k}]^A, \end{aligned} \quad (71)$$

which depends on the scattering matrix parameters only via the elementary scattering event  $[x'_{kk'}]^K$ . Analogous relations hold for  $\tilde{X}_p^K$ .

The transport equation for the distribution function is solved by any function of energy in equilibrium. The correct boundary conditions in this case are

$$x^{(\text{eq})} = (1 - \gamma^R \tilde{\gamma}^A) \tanh\left(\frac{\varepsilon - q\Phi}{2k_B T}\right), \quad \tilde{x}^{(\text{eq})} = -(1 - \tilde{\gamma}^R \gamma^A) \tanh\left(\frac{\varepsilon + q\Phi}{2k_B T}\right) \quad (72)$$

for excitations of charge  $q$  in an electrostatic potential  $\Phi$ .

### 3.6.3 Case 1: one-trajectory scattering

In this case only one incoming and one outgoing trajectory are coupled via the boundary conditions. The corresponding normal state scattering matrix is denoted by  $S$  and is a scalar in trajectory space. The boundary conditions read in this case simply

$$[\gamma']^R = S^R \circ \gamma^R \circ \tilde{S}^R, \quad \Gamma^R = [\gamma']^R, \quad (73)$$

and

$$[x']^K = S^R \circ x^K \circ S^A, \quad X_k^K = [x']^K. \quad (74)$$

### 3.6.4 Case 2: two-trajectory scattering

This is the case of scattering from two incoming trajectories into two outgoing trajectories. Examples are reflection and transmission at an interface, or reflection from a surface in a two-band system. The scattering matrix and the elementary scattering events have in this case the form

$$S = \begin{pmatrix} S_{11} & S_{12} \\ S_{21} & S_{22} \end{pmatrix}, \quad [\gamma'_{ij}]^R = \sum_{l=1,2} S_{il}^R \circ \gamma_l^R \circ \tilde{S}_{lj}^R, \quad [x'_{ij}]^K = \sum_{l=1,2} S_{il}^R \circ x_l^K \circ S_{lj}^A. \quad (75)$$

We give the solutions for trajectory 1, the remaining solution can be obtained by interchanging the indices 1 and 2. The boundary conditions read for  $i, j = 1, 2$

$$\Gamma_{1\leftarrow 1}^R = [\gamma'_{11} + \Gamma_{1\leftarrow 2} \circ \tilde{\gamma}_2 \circ \gamma'_{21}]^R, \quad \Gamma_{1\leftarrow 2}^R = [\gamma'_{12} + \Gamma_{1\leftarrow 2} \circ \tilde{\gamma}_2 \circ \gamma'_{22}]^R. \quad (76)$$

The equation for the  $\Gamma_{1\leftarrow 2}$  can be solved by simple inversion,

$$\Gamma_{1\leftarrow 2}^R = [\gamma'_{12} \circ (1 - \tilde{\gamma}_2 \circ \gamma'_{22})^{-1}]^R, \quad (77)$$

and the solution introduced into the equation for  $\Gamma_{1\leftarrow 1}^R = \Gamma_1^R$ ,

$$\Gamma_1^R = [\gamma'_{11} + \gamma'_{12} \circ (1 - \tilde{\gamma}_2 \circ \gamma'_{22})^{-1} \circ \tilde{\gamma}_2 \circ \gamma'_{21}]^R. \quad (78)$$

For the distribution function one needs the components  $\bar{\Gamma}_{1\leftarrow 2}^R = \Gamma_{1\leftarrow 2}^R$  and obtains

$$\begin{aligned} X_1^K &= [x'_{11}]^K + \Gamma_{1\leftarrow 2}^R \circ \tilde{\gamma}_2^R \circ [x'_{21}]^K + [x'_{12}]^K \circ \gamma_2^A \circ \tilde{\Gamma}_{2\rightarrow 1}^A \\ &\quad + \Gamma_{1\leftarrow 2}^R \circ \left( \tilde{\gamma}_2^R \circ [x'_{22}]^K \circ \gamma_2^A - \tilde{x}_2^K \right) \circ \tilde{\Gamma}_{2\rightarrow 1}^A. \end{aligned} \quad (79)$$

We present here formulas for the special case of the zero temperature conductance when a single band system is contacted by a normal metal. We assign the index 1 to the normal metal side of the interface and the index 2 to the superconducting side. The momentum for incoming trajectories on the superconducting side of the interface is denoted by  $\mathbf{k}_2$ , and that for the outgoing trajectory on the superconducting side by  $\tilde{\mathbf{k}}_2$ . For the normal side the corresponding momenta are  $\mathbf{k}_1$  and  $\tilde{\mathbf{k}}_1$  (see Fig. 8 for the scattering geometry). The projection on the interface of all four momenta is equal. The corresponding incoming coherence functions in the superconductor are  $\gamma_2(\varepsilon) \equiv \gamma_2^R(\mathbf{k}_2, \varepsilon)$  and  $\tilde{\gamma}_2(\varepsilon) \equiv \tilde{\gamma}_2^R(\tilde{\mathbf{k}}_2, \varepsilon)$ . Furthermore,  $S_{12} \equiv S_{12}^R(\tilde{\mathbf{k}}_1, \mathbf{k}_2)$ ,  $S_{22} \equiv S_{22}^R(\mathbf{k}_2, \mathbf{k}_2)$ , and  $\tilde{S}_{22} = \tilde{S}_{22}^R(\mathbf{k}_2, \tilde{\mathbf{k}}_2)$ . The Fermi velocity for outgoing directions on the normal side will be denoted by  $\mathbf{v}_{F1} \equiv \mathbf{v}_{F1}(\tilde{\mathbf{k}}_1)$ . Having thus specified all momentum dependencies, we will suppress in the formulas below the momentum variables. In the case under consideration, after introducing Eqs. (77), (78), and (79) into Eq. (53), we obtain after some algebra (we omit hereafter the  $\circ$  sign)

$$\begin{aligned} \frac{G(eV)}{G_N} = & \left\langle \hat{\mathbf{n}}\mathbf{v}_{F1} \left\{ \left| |S_{12}[1 + A_2(\varepsilon)S_{22}]|^2 - |S_{12}A_2(\varepsilon)|^2 \right\} \right\}_{\varepsilon=eV}^+ \right. \\ & \left. + \left\langle \hat{\mathbf{n}}\mathbf{v}_{F1} \left| |S_{12}[1 + A_2(\varepsilon)S_{22}]\gamma_2(\varepsilon)\tilde{S}_{21}|^2 \right| \right\}_{\varepsilon=-eV}^+ \right. \end{aligned} \quad (80)$$

where

$$A_2(\varepsilon) = \left( 1 - \gamma_2(\varepsilon)\tilde{S}_{22}\tilde{\gamma}_2(\varepsilon)S_{22} \right)^{-1} \gamma_2(\varepsilon)\tilde{S}_{22}\tilde{\gamma}_2(\varepsilon) \quad (81)$$

and we used the notation  $\|A\|^2 = \frac{1}{2}\text{Tr}(AA^\dagger)$  for any  $2 \times 2$  matrix  $A$ . The symbol  $\langle \dots \rangle_{\varepsilon=eV}^+$  denotes Fermi surface average only over outgoing directions, and the argument is to be taken at energy  $eV$ . For  $S_{22} = \tilde{S}_{22} = -\sqrt{R(\theta)}$ ,  $S_{12} = \tilde{S}_{21} = \sqrt{D(\theta)}$  (with impact angle  $\theta$ ), Eq. (80) reduces to Eq. (10). For the tunneling limit we can neglect the second line in Eq. (80), and using the relation

$$1 + A_2(\varepsilon)S_{22} = \frac{1}{2} \{ \mathcal{N}_2(\varepsilon) + 1 \} \quad (82)$$

with the complex quantity

$$\mathcal{N}_2(\varepsilon) = \left\{ \left( 1 - \gamma_2(\varepsilon)\tilde{S}_{22}\tilde{\gamma}_2(\varepsilon)S_{22} \right)^{-1} \left( 1 + \gamma_2(\varepsilon)\tilde{S}_{22}\tilde{\gamma}_2(\varepsilon)S_{22} \right) \right\}$$

the conductance simplifies after some re-arrangements to

$$\frac{G(eV)}{G_N} = \frac{1}{2} \text{ReTr} \left\langle \hat{\mathbf{n}}\mathbf{v}_{F1} \left\{ S_{12} \mathcal{N}_2(eV) (S_{12})^\dagger \right\} \right\rangle^+. \quad (83)$$

For the tunneling limit, in  $\mathcal{N}_2$  the surface scattering matrix (i.e. for  $S_{12} = S_{21} = 0$ ) can be used, for which the local density of states at an impenetrable surface is

$$\frac{N_2(\varepsilon)}{N_{2,F}} = \frac{1}{2} \text{ReTr} \left\langle \mathcal{N}_2(\varepsilon) + S_{22} \mathcal{N}_2(\varepsilon) S_{22}^\dagger \right\rangle^+. \quad (84)$$

### 3.6.5 Scattering matrix for non-centrosymmetric/normal-metal junction

For the case that a non-centrosymmetric material with small spin-orbit splitting is brought in contact with a normal metal, we can use the formulas of the last subsection. The scattering matrix for scattering between the two helicity bands in the non-centrosymmetric metal (index 2) and the two spin bands in the normal metal (index 1) can be expressed in terms of the scattering matrix for scattering between spin states on both sides of the interface. The corresponding transformation is

$$\begin{pmatrix} S'_{11} & S'_{12} \\ S'_{21} & S'_{22} \end{pmatrix} = \begin{pmatrix} 1 & 0 \\ 0 & U_{\mathbf{k}} \end{pmatrix} \cdot \begin{pmatrix} S_{11} & S_{12} \\ S_{21} & S_{22} \end{pmatrix} \cdot \begin{pmatrix} 1 & 0 \\ 0 & U_{\mathbf{k}}^\dagger \end{pmatrix}, \quad (85)$$

$$\begin{pmatrix} \tilde{S}'_{11} & \tilde{S}'_{12} \\ \tilde{S}'_{21} & \tilde{S}'_{22} \end{pmatrix} = \begin{pmatrix} 1 & 0 \\ 0 & U_{-\mathbf{k}}^* \end{pmatrix} \cdot \begin{pmatrix} \tilde{S}_{11} & \tilde{S}_{12} \\ \tilde{S}_{21} & \tilde{S}_{22} \end{pmatrix} \cdot \begin{pmatrix} 1 & 0 \\ 0 & U_{-\mathbf{k}}^T \end{pmatrix}. \quad (86)$$

For the simple case of a spin-conserving scattering in the spin/spin representation, the spin/helicity representation of the scattering matrix takes the form

$$\begin{pmatrix} S'_{11} & S'_{12} \\ S'_{21} & S'_{22} \end{pmatrix} = \begin{pmatrix} r & t U_{\mathbf{k}}^\dagger \\ t^* U_{\mathbf{k}} & -r U_{\mathbf{k}} U_{\mathbf{k}}^\dagger \end{pmatrix}, \quad \begin{pmatrix} \tilde{S}'_{11} & \tilde{S}'_{12} \\ \tilde{S}'_{21} & \tilde{S}'_{22} \end{pmatrix} = \begin{pmatrix} r & t^* U_{-\mathbf{k}}^T \\ t U_{-\mathbf{k}}^* & -r U_{-\mathbf{k}}^* U_{-\mathbf{k}}^T \end{pmatrix}. \quad (87)$$

where  $r \equiv r_{\mathbf{k}\mathbf{k}}$  and  $t = t_{\mathbf{k}\mathbf{k}}$  with  $r^2 + |t|^2 = 1$  are reflection and transmission coefficients that depend on the (conserved) momentum projection on the interface. We have chosen  $r$  real, as in quasiclassical approximation possible reflection phases do not affect the results. The case  $t = 0$  can be used to describe scattering at a surface.

In the case of a contact with a non-centrosymmetric metal with strong spin-orbit split bands the scattering matrix has a more complicated structure. It connects in this case three incoming with three outgoing trajectories, and the scattering at the interface will not be spin-conserving. For this case, it does then not make sense anymore do use a spin/spin representation, but a spin/helicity representation must be used consistently. The scattering matrix must be obtained in agreement with the symmetry group of the interface, and it cannot in general be related anymore to the  $U_{\mathbf{k}}$  matrices in a simple way.

### 3.7 Superconducting order parameter

For the case of weak spin-orbit splitting one expects that to leading order in the small expansion parameters either a singlet or a triplet component nucleates. On the other hand, any finite spin-orbit interaction leads to a mixture of spin singlet ( $\Delta_s$ ) and triplet ( $\Delta_t$ ) components [89,90]. Consequently, the singlet or triplet states are never pure, but they are mixed. This mixing becomes in particular prominent when the spin-orbit interaction is strong. In this case, it does not make sense anymore to speak about singlet or triplet components, but it is necessary to start from the helicity basis.

It is interesting to consider what happens in the weak case first. In this case the triplet component is expected to be induced directly by the structure of the spin-orbit interaction, and the spin triplet component aligns with  $\mathbf{g}(\mathbf{k})$ . The gap function is in this case in spin representation given by,

$$\Delta^s = (\Delta_{\mathbf{k}} + D_{\mathbf{k}} \mathbf{g}(\mathbf{k}) \cdot \boldsymbol{\sigma}) i\sigma^{(2)} \quad (88)$$

which transforms in helicity basis into

$$\begin{aligned} \Delta &= U_{\mathbf{k}} (\Delta_{\mathbf{k}} + D_{\mathbf{k}} \mathbf{g}(\mathbf{k}) \cdot \boldsymbol{\sigma}) i\sigma^{(2)} U_{-\mathbf{k}}^T \\ &= U_{\mathbf{k}} (\Delta_{\mathbf{k}} + D_{\mathbf{k}} \mathbf{g}(\mathbf{k}) \cdot \boldsymbol{\sigma}) U_{\mathbf{k}}^\dagger U_{\mathbf{k}} i\sigma^{(2)} U_{-\mathbf{k}}^T \\ &= (\Delta_{\mathbf{k}} + D_{\mathbf{k}} |\mathbf{g}(\mathbf{k})| \sigma^{(3)}) U_{\mathbf{k}} U_{-\mathbf{k}}^\dagger i\sigma^{(2)}. \end{aligned} \quad (89)$$

We introduce the notation

$$(U_{\mathbf{k}} U_{-\mathbf{k}}^\dagger)_{\lambda\lambda'} = \begin{pmatrix} 0 & e^{-i\phi_{\mathbf{g}}} \\ -e^{i\phi_{\mathbf{g}}} & 0 \end{pmatrix} \equiv -i\sigma_{\lambda\lambda'}^{(\mathbf{g})}. \quad (90)$$

Note that the identities  $(\sigma^{(\mathbf{g})})^2 = 1$ ,  $\sigma^{(-\mathbf{g})} = -\sigma^{(\mathbf{g})}$ , and  $\sigma^{(2)} \sigma^{(\mathbf{g})} \sigma^{(2)} = -\sigma^{(\mathbf{g})}$ , hold. With this, we can obtain the Nambu-Gor'kov space structure of the order parameter

$$\begin{aligned} \hat{\Delta} &= \begin{pmatrix} 0 & \Delta \\ \tilde{\Delta} & 0 \end{pmatrix} = \begin{pmatrix} 0 & (\Delta_{\mathbf{k}} + D_{\mathbf{k}} |\mathbf{g}(\mathbf{k})| \sigma^{(3)}) \sigma^{(\mathbf{g})} \sigma^{(2)} \\ (\Delta_{-\mathbf{k}} + D_{-\mathbf{k}} |\mathbf{g}(\mathbf{k})| \sigma^{(3)})^* \sigma^{(\mathbf{g})} \sigma^{(2)} & 0 \end{pmatrix} \\ &= \begin{pmatrix} 0 & (\Delta_{\mathbf{k}} + D_{\mathbf{k}} |\mathbf{g}(\mathbf{k})| \sigma^{(3)}) i\sigma^{(2)} \\ (\Delta_{\mathbf{k}}^* + D_{\mathbf{k}}^* |\mathbf{g}(\mathbf{k})| \sigma^{(3)}) i\sigma^{(2)} & 0 \end{pmatrix} \begin{pmatrix} i\sigma^{(\mathbf{g})} & 0 \\ 0 & -i\sigma^{(-\mathbf{g})} \end{pmatrix}, \end{aligned} \quad (91)$$

where  $\Delta_{-\mathbf{k}} = \Delta_{\mathbf{k}}$ , and  $D_{-\mathbf{k}} = D_{\mathbf{k}}$ , and we have used  $\sigma^{(\mathbf{g})} \sigma^{(3)} \sigma^{(\mathbf{g})} = -\sigma^{(3)}$ . With  $\Delta_{\pm}(\mathbf{k}) = \Delta_{\mathbf{k}} \pm D_{\mathbf{k}} |\mathbf{g}(\mathbf{k})|$  the order parameter can be cast in the form

$$\Delta(\mathbf{k}) = \begin{pmatrix} \Delta_+(\mathbf{k}) t_+(\mathbf{k}) & 0 \\ 0 & \Delta_-(\mathbf{k}) t_-(\mathbf{k}) \end{pmatrix} \quad (92)$$

$$\tilde{\Delta}(\mathbf{k}) = \begin{pmatrix} \Delta_+(\mathbf{k})^* t_+(-\mathbf{k})^* & 0 \\ 0 & \Delta_-(\mathbf{k})^* t_-(-\mathbf{k})^* \end{pmatrix}. \quad (93)$$

with phase factors  $t_\lambda(\mathbf{k}) = -e^{-i\lambda\phi_{\mathbf{g}}}$ . Note that  $t_\lambda(-\mathbf{k}) = -t_\lambda(\mathbf{k})$ , and  $|t_\lambda(\mathbf{k})| = 1$ , and  $\Delta_{\pm}(-\mathbf{k}) = \Delta_{\pm}(\mathbf{k})$ .

We note that other possibilities to define the canonical transformation that diagonalizes the kinetic part of the Hamiltonian exist, which differ by the relation between particle and hole components. Using these alternative definitions (e.g. in Refs. [36, 44]), the order parameter is purely off-diagonal instead of diagonal in the band representation, and the symmetry relation Eq. (59) becomes non-trivial (see e.g. Ref. [44]). Here, we prefer a transformation that preserves the symmetry (59), and renders the order parameter above diagonal. This is a natural choice when treating strongly spin-orbit split systems, where the order parameter should be band diagonal.

The coherence amplitudes in a bulk system with order parameter Eq. (92) are of a similar form,

$$\gamma(\mathbf{k}, \varepsilon) = \begin{pmatrix} \gamma_+(\mathbf{k}, \varepsilon) t_+(\mathbf{k}) & 0 \\ 0 & \gamma_-(\mathbf{k}, \varepsilon) t_-(\mathbf{k}) \end{pmatrix} \quad (94)$$

$$\tilde{\gamma}(\mathbf{k}, \varepsilon) = \begin{pmatrix} \tilde{\gamma}_+(\mathbf{k}, \varepsilon) t_+(-\mathbf{k})^* & 0 \\ 0 & \tilde{\gamma}_-(\mathbf{k}, \varepsilon) t_-(-\mathbf{k})^* \end{pmatrix} \quad (95)$$

with  $\tilde{\gamma}_\pm(\mathbf{k}, \varepsilon) = \gamma_\pm(-\mathbf{k}, -\varepsilon)^*$ . In inhomogeneous systems helicity-mixing can take place. If this happens, the form of the coherence functions is the same band-diagonal form as above for the case of strong spin-orbit splitting, however has the full matrix structure for the case of weak spin-orbit splitting.

### 3.8 Results

#### 3.8.1 Andreev bound states near the surface

The surface bound states are determined by the poles of the Green's function. Following Refs. [42, 44], we consider specular reflection, whereby the component of  $\mathbf{k}$  normal to surface changes sign,  $\mathbf{k} \rightarrow \underline{\mathbf{k}}$ , whereas the component parallel to the surface is conserved. We find the amplitudes  $\gamma(\mathbf{k}, \varepsilon)$  by integrating forward along the incoming,  $\mathbf{k}$ , trajectory starting from the values in the bulk, and the amplitudes  $\tilde{\gamma}(\underline{\mathbf{k}}, \varepsilon)$  by integrating backward along the outgoing,  $\underline{\mathbf{k}}$ , trajectory, again starting from the values in the bulk [20]. For the homogeneous solutions one obtains

$$\gamma_\pm^0(\mathbf{k}, \varepsilon) = -\frac{\Delta_\pm(\mathbf{k})}{\varepsilon + i\sqrt{|\Delta_\pm(\mathbf{k})|^2 - \varepsilon^2}}, \quad \tilde{\gamma}_\pm^0(\underline{\mathbf{k}}, \varepsilon) = \frac{\Delta_\pm(\underline{\mathbf{k}})^*}{\varepsilon + i\sqrt{|\Delta_\pm(\underline{\mathbf{k}})|^2 - \varepsilon^2}}, \quad (96)$$

Note that the spin-orbit interaction in the helicity basis enters as a term proportional to  $\sigma^{(3)}$ , see Eq. (55). Consequently, this term commutes with any term diagonal in the helicity basis, and thus drops out of the homogeneous solutions in Eq. (96) (see Ref. [91] for the case of a Rashba-type spin-orbit coupling). Note, however, that this is not in general the case for non-homogeneous solutions: when helicity mixing takes place due to impurities or surfaces and interfaces, and a fully self-consistent solution is obtained, then the spin-orbit coupling term in Eq. (55) enters through the transport equation.

The amplitudes  $\Gamma_{\underline{\mathbf{k}}}$  and  $\tilde{\Gamma}_{\mathbf{k}}$ , are determined from the boundary conditions at the surface. We consider here a simple model of a non-magnetic surface, that conserves the spin under reflection (this assumption only holds for a *small* spin-orbit interaction in the bulk material). In this case the components of  $\hat{g}$  in the spin basis,

$$\hat{g}^s(\mathbf{k}, \varepsilon) = \hat{U}_{\mathbf{k}}^\dagger \hat{g}(\mathbf{k}, \varepsilon) \hat{U}_{\mathbf{k}}, \quad (97)$$

are continuous at the surface. This leads to a surface induced mixing of the helicity bands according to

$$U_{\underline{\mathbf{k}}}^\dagger \Gamma(\underline{\mathbf{k}}, \varepsilon) U_{-\underline{\mathbf{k}}}^* = \Gamma^s(\underline{\mathbf{k}}, \varepsilon) = \gamma^s(\mathbf{k}, \varepsilon) = U_{\underline{\mathbf{k}}}^\dagger \gamma(\mathbf{k}, \varepsilon) U_{-\mathbf{k}}, \quad (98)$$

$$U_{-\mathbf{k}}^T \tilde{\Gamma}(\mathbf{k}, \varepsilon) U_{\mathbf{k}} = \tilde{\Gamma}^s(\mathbf{k}, \varepsilon) = \tilde{\gamma}^s(\underline{\mathbf{k}}, \varepsilon) = U_{-\underline{\mathbf{k}}}^T \tilde{\gamma}(\underline{\mathbf{k}}, \varepsilon) U_{\underline{\mathbf{k}}}. \quad (99)$$

Note that these boundary conditions correspond to Eq. (73) with  $S^R$  and  $\tilde{S}^R$  given by the (22)-components of Eq. (87).

We proceed with discussing the local density of states at the surface,  $N(\varepsilon)$ , that is defined in terms of the momentum resolved density of states,  $N(\mathbf{k}, \varepsilon)$  by

$$N(\mathbf{k}, \varepsilon)/N_F = -(2\pi)^{-1} \text{ImTr}_\lambda \{g(\mathbf{k}, \varepsilon)\}, \quad N(\varepsilon) = \langle N(\mathbf{k}, \varepsilon) \rangle, \quad (100)$$

which can be expressed in terms of the coherence amplitudes in the following way (here  $\mathbf{k}$  points towards the surface and  $\underline{\mathbf{k}}$  away from it),

$$\begin{aligned} N(\mathbf{k}, \varepsilon)/N_F &= \text{ReTr}_\lambda \left\{ [1 - \gamma(\mathbf{k}, \varepsilon) \tilde{\Gamma}(\mathbf{k}, \varepsilon)]^{-1} - 1/2 \right\} \\ N(\underline{\mathbf{k}}, \varepsilon)/N_F &= \text{ReTr}_\lambda \left\{ [1 - \Gamma(\underline{\mathbf{k}}, \varepsilon) \tilde{\gamma}(\underline{\mathbf{k}}, \varepsilon)]^{-1} - 1/2 \right\}. \end{aligned} \quad (101)$$

We obtain  $\Gamma(\underline{\mathbf{k}}, \varepsilon)$  and  $\tilde{\Gamma}(\mathbf{k}, \varepsilon)$  from Eqs. (98) and (99), with  $\gamma(\mathbf{k}, \varepsilon)$  and  $\tilde{\gamma}(\underline{\mathbf{k}}, \varepsilon)$  from Eqs. (94), (95), (96), and (105).

The bound states in the surface density of states correspond to the zero eigenvalues of the matrix

$$1 - \gamma(\mathbf{k}, \varepsilon) \tilde{\Gamma}(\mathbf{k}, \varepsilon) = 1 - \gamma(\mathbf{k}, \varepsilon) (U_{-\mathbf{k}}^* U_{\mathbf{k}}^T) \tilde{\gamma}(\underline{\mathbf{k}}, \varepsilon) (U_{\underline{\mathbf{k}}} U_{\underline{\mathbf{k}}}^\dagger) \quad (102)$$

at the surface. An explicit calculation results in an equation for the Andreev bound states energy in terms of the surface coherence amplitudes in the helicity basis [44],

$$\frac{\{1 + \gamma_+ \tilde{\gamma}_+\} \{1 + \gamma_- \tilde{\gamma}_-\}}{\{1 + \gamma_+ \tilde{\gamma}_-\} \{1 + \gamma_- \tilde{\gamma}_+\}} = -\mathcal{M}, \quad (103)$$

where we used the abbreviations  $\gamma_\pm \equiv \gamma_\pm(\mathbf{k}, \varepsilon)$  and  $\tilde{\gamma}_\pm \equiv \tilde{\gamma}_\pm(\underline{\mathbf{k}}, \varepsilon)$ . The ‘‘mixing’’ factor  $\mathcal{M}$  is determined by the change of  $\mathbf{g}(\mathbf{k}) \rightarrow \mathbf{g}(\underline{\mathbf{k}})$  under reflection  $\mathbf{k} \rightarrow \underline{\mathbf{k}}$  at the surface,

$$\mathcal{M} = \frac{\sin^2 \frac{\theta_{\underline{\mathbf{g}}} - \theta_{\mathbf{g}}}{2} + \sin^2 \frac{\theta_{\underline{\mathbf{g}}} + \theta_{\mathbf{g}}}{2} \tan^2 \frac{\varphi_{\underline{\mathbf{g}}} - \varphi_{\mathbf{g}}}{2}}{\cos^2 \frac{\theta_{\underline{\mathbf{g}}} - \theta_{\mathbf{g}}}{2} + \cos^2 \frac{\theta_{\underline{\mathbf{g}}} + \theta_{\mathbf{g}}}{2} \tan^2 \frac{\varphi_{\underline{\mathbf{g}}} - \varphi_{\mathbf{g}}}{2}}, \quad (104)$$

where  $\theta_{\mathbf{g}}, \varphi_{\mathbf{g}}$  and  $\theta_{\underline{\mathbf{g}}}, \varphi_{\underline{\mathbf{g}}}$  are the polar and azimuthal angles of  $\mathbf{g}(\mathbf{k})$  and  $\mathbf{g}(\underline{\mathbf{k}})$ , respectively.

In general, the order parameter must be obtained self-consistently at the surface. Helicity mixing at the surface will lead necessarily to a suppression of the order parameter. To gain insight in the role of the order parameter suppression it is useful to model it by a normal layer of width  $W$  next to the interface. Trajectories incident at an angle  $\alpha_{\mathbf{k}}$  from the surface normal travel through a normal region of an effective width  $2W_{\mathbf{k}} = 2W / \cos(\alpha_{\mathbf{k}})$ . Thus, the surface coherence amplitudes gain a phase factor,

$$\gamma_\pm(\mathbf{k}, \varepsilon) = \gamma_\pm^0(\mathbf{k}, \varepsilon) e^{2i\varepsilon W / v_F \cos(\alpha_{\mathbf{k}})}, \quad \tilde{\gamma}_\pm(\underline{\mathbf{k}}, \varepsilon) = \tilde{\gamma}_\pm^0(\underline{\mathbf{k}}, \varepsilon) e^{2i\varepsilon W / v_F \cos(\alpha_{\mathbf{k}})}. \quad (105)$$



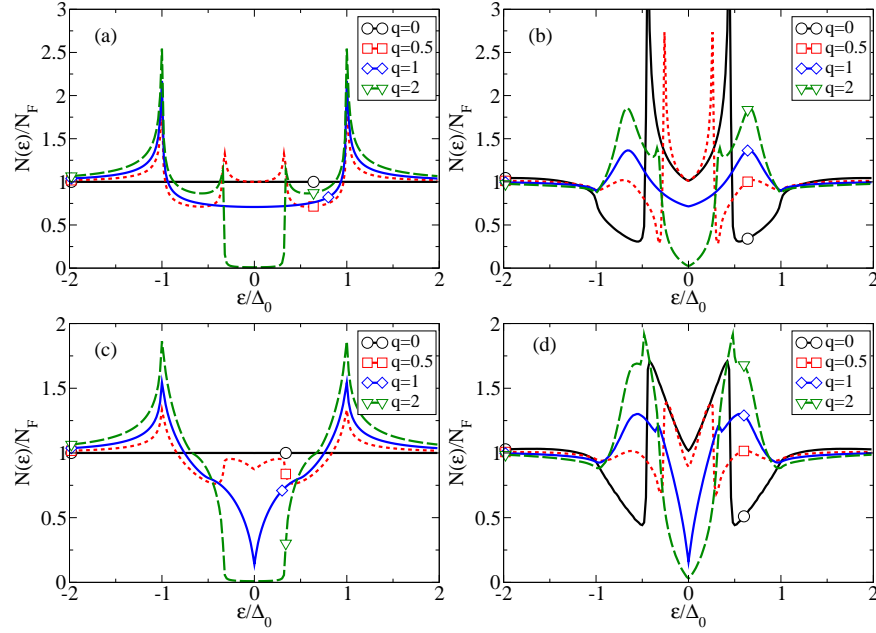


**Fig. 9** (Color online) Local surface density of states  $N(\varepsilon)/N_F$  for a Rashba superconductor,  $\mathbf{g}(\mathbf{k}) = \alpha_R \mathbf{k} \times \hat{z}$ . The surface is parallel to  $\hat{z}$ . The curves are for  $\Delta_{\pm} = \Delta_0(q \pm |\hat{\mathbf{g}}(\mathbf{k})|)/(q+1)$ , with  $q$  ranging from 0 to 2. In (a) and (c) the order parameter is assumed constant up to the surface, and in (b) and (d) a suppression of the order parameter to zero in a surface layer of thickness  $W = 2\xi_0$  with  $\xi_0 = \hbar v_F / 2\pi k_B T_c$  is assumed. (a) and (b) is for a cylindrical Fermi surface,  $\mathbf{v}_F = (v_x, v_y, 0)$ , and (c) and (d) is for a spherical Fermi surface. (The symbols are labels for the curves only).

Similarly like for  $\mathbf{g}$  we will use in the following polar and azimuthal angles for the vector  $\mathbf{k}$ , defined by  $\{k_x, k_y, k_z\} = |\mathbf{k}| \{\sin(\theta_{\mathbf{k}}) \cos(\varphi_{\mathbf{k}}), \sin(\theta_{\mathbf{k}}) \sin(\varphi_{\mathbf{k}}), \cos(\theta_{\mathbf{k}})\}$  (where  $0 \leq \theta_{\mathbf{k}} \leq \pi$ ). We also introduce the notation  $\hat{\mathbf{g}} = \mathbf{g} / \max(|\mathbf{g}|)$ . For the order parameter, we assume isotropic  $\Delta_{\mathbf{k}} = \Delta$  and  $D_{\mathbf{k}} = D$  in Eq. (88), and introduce the parameter  $q = \Delta / D'$  where  $D' = D \cdot \max(|\mathbf{g}|)$  [42]. In this case  $\Delta_{\pm} = D'(q \pm |\hat{\mathbf{g}}|)$  with maximal gap amplitudes  $\Delta_0 = D'(q+1)$ .

In Fig. 9 we show results for a Rashba-type spin-orbit coupling,  $\mathbf{g}(\mathbf{k}) = \alpha_R \mathbf{k} \times \hat{z}$ . The surface is aligned with the  $\hat{z}$  direction. In (a) and (b) we use a cylindrical Fermi surface, for which  $|\hat{\mathbf{g}}(\mathbf{k})| = 1$ . In (c) and (d) the results for a spherical Fermi surface are shown, for which  $|\hat{\mathbf{g}}(\mathbf{k})| = \sin(\theta_{\mathbf{k}})$ . The effect of a surface layer with suppressed order parameter is illustrated in Fig. 9 (b) and (d), where Eq. (105) with  $W = 2\xi_0$  is used, where  $\xi_0$  is the coherence length  $\xi_0 = \hbar v_F / 2\pi k_B T_c$ .

For the special case  $q = 0$  we have  $\Delta_+ = -\Delta_- = \Delta_0 \sin(\theta_{\mathbf{k}})$  (we use a real gauge). For this case,  $\theta_{\mathbf{g}} = \theta_{\hat{\mathbf{g}}} = \pi/2$ , and consequently,  $\mathcal{M} = \tan^2 \varphi_{\mathbf{g}} = \cot^2 \varphi_{\mathbf{k}}$ . The bound states are then given by [42, 44]

$$\frac{\varepsilon}{\Delta_0} = -\sin\left(\frac{2W\varepsilon}{v_F \cos \varphi_{\mathbf{k}}} \pm \varphi_{\mathbf{k}}\right) \sin(\theta_{\mathbf{k}}). \quad (106)$$

Numerical solution of the problem shows that the ‘‘principal’’ bound state branches  $\varepsilon(\varphi_{\mathbf{k}})$  with energies away from the continuum edge contribute the most to the sub-gap DOS. For  $W \neq 0$  the main branch  $\varepsilon_{bs}(\varphi_{\mathbf{k}})$  develops a maximum at  $\varepsilon^* < \Delta_0$ , which gives rise to a peak in the surface DOS near  $\varepsilon^*$ , see Fig. 9 (b) and (d). Fully self-consistent solution confirms this [44]. For  $q \rightarrow \infty$  the order parameter becomes insensitive to helicity mixing, i.e. the effective  $W$  decreases for increasing  $q$ .

Andreev bound states in non-centrosymmetric superconductors have unusual spin structure [40,44]. It is found, that the states corresponding to different branches of Eq. (106) have opposite spin polarization. Since the spin polarization changes sign for reversed trajectories, the Andreev states carry spin current along the interface. Such spin currents exist in NCS materials because the spin is not conserved, and consequently precession terms enter the continuity equation [92]. There are spin currents both in the normal state and in the superconducting state. As was found in Ref. [44], the most prominent feature is a large surface current with out of plane spin polarization (reminiscent to that in spin Hall bars [93]) that flows along the surface, and decays rapidly into the bulk on a Fermi wavelength scale. In addition, there is also a surface induced superconducting spin current with out of plane spin polarization, that adds to the background microscopic spin currents and greatly exceeds them in the limit of small spin-orbit band splitting. This effect is in this case solely determined by the structure of the superconducting gap. Superconducting spin currents decay into the bulk on the scale of the coherence length and show oscillations determined by the spin-orbit strength due to Faraday-like rotations of the spin coherence functions along quasiparticle trajectories [44].

### 3.8.2 Tunneling conductance

For a three-dimensional model, which for the Rashba-type spin-orbit coupling was discussed in Ref. [42], we present in the following tunneling conductances in various geometries. We will discuss several types of spin-orbit interaction:

$$\begin{aligned} C_{4v}: \quad \mathbf{g} &= \eta \begin{pmatrix} \hat{k}_y \\ -\hat{k}_x \\ 0 \end{pmatrix} + \eta' \begin{pmatrix} \hat{0} \\ 0 \\ \hat{k}_x \hat{k}_y \hat{k}_z (\hat{k}_x^2 - \hat{k}_y^2) \end{pmatrix}, \\ T_d: \quad \mathbf{g} &= \eta \begin{pmatrix} \hat{k}_x (\hat{k}_y^2 - \hat{k}_z^2) \\ \hat{k}_y (\hat{k}_z^2 - \hat{k}_x^2) \\ \hat{k}_z (\hat{k}_x^2 - \hat{k}_y^2) \end{pmatrix}, \quad O: \quad \mathbf{g} = \eta \begin{pmatrix} \hat{k}_x \\ \hat{k}_y \\ \hat{k}_z \end{pmatrix}, \end{aligned} \quad (107)$$

For the symmetry  $C_{4v}$ , corresponding to the tetragonal point group, the two parameters  $\eta$  and  $\eta'$  can both be non-zero. We will discuss below the special cases  $\eta = 0$  and  $\eta' = 0$ . The case  $\eta' = 0$  corresponds to a Rashba spin-orbit coupling. The type of spin-orbit coupling we consider for the full tetrahedral point group,  $T_d$ , is also known as Dresselhaus coupling. Finally, for the cubic point group,  $O$ , the simplest form for  $\mathbf{g}$  is considered here, which is fully isotropic. All the cases above

are relevant for non-centrosymmetric superconductors:  $C_{4v}$  for CePt<sub>3</sub>Si, CeRhSi<sub>3</sub>, and CeIrSi<sub>3</sub>,  $T_d$  for Y<sub>2</sub>C<sub>3</sub> and possibly KOs<sub>2</sub>O<sub>6</sub>, and O for Li<sub>2</sub>(Pd<sub>1-x</sub>Pt<sub>x</sub>)<sub>3</sub>B.

The zero temperature tunneling conductance is obtained according to the formula Eq. (83), which leads for a spin-inactive  $\delta$ -function barrier to

$$\frac{G(eV)}{G_N} = \frac{\langle \cos(\alpha_{\mathbf{k}}) D(\alpha_{\mathbf{k}}) N(\mathbf{k}, eV) \rangle}{\langle \cos(\alpha_{\mathbf{k}}) D(\alpha_{\mathbf{k}}) \rangle}, \quad D(\alpha_{\mathbf{k}}) = \frac{D_0 \cos^2(\alpha_{\mathbf{k}})}{1 - D_0 \sin^2(\alpha_{\mathbf{k}})} \quad (108)$$

where  $\alpha_{\mathbf{k}}$  is the angle between the surface normal and  $\mathbf{k}$ . A remark is in place here. In principle, the interface barrier will be spin-dependent once a spin-orbit split material is brought in contact with a normal metal. However, for the limit of small spin-orbit splitting we can neglect the spin-dependence of the interface potential consistent with the quasiclassical approximation. The corrections are of the same order as the corrections for the quasiparticle velocity in this case, and are of higher order in the parameter SMALL.

In Figure. 10 we show the tunneling conductance  $G(eV)/G_N$  obtained from Eq. (108) with Eqs. (100)-(101) for various types of spin-orbit coupling corresponding to the spin-orbit couplings in Eq. (107), and for various alignments of the surface normal with respect to the crystal symmetry directions. The tunneling parameter in this figure is  $D_0 = 0.1$ . We show curves for an order parameter  $\Delta_{\pm} = \Delta_0(q \pm |\hat{\mathbf{g}}(\mathbf{k})|)/(q+1)$ , with  $q$  ranging from 0 to 2. For simplicity, we concentrate here on the assumption that the order parameter is constant up to the surface, i.e. we use the bulk solutions Eqs. (94)-(96). For a detailed quantitative description, a self-consistent determination of the order parameter suppression near the surface must be obtained. We also use the simplifying assumptions of a spherical Fermi surface with isotropic Fermi velocity.

As seen from Fig. 10, a rich structure of Andreev bound states below the bulk gap energy develops, that depends strongly on the alignment of the surface with the crystal symmetry axes. In (a) and (b) a pure Rashba spin-orbit coupling  $\mathbf{k} = [\hat{k}_y, -\hat{k}_x, 0]$  on a Fermi sphere is assumed. Below the critical value  $q = 1$ , a zero bias peak appears for tunneling in the direction perpendicular to the  $\hat{z}$  direction, i.e. the (1,0,0) or (0,1,0) direction, however a dependence quadratic in energy appears for tunneling parallel to the  $\hat{z}$  direction, i.e. the (0,0,1) direction [42]. For  $q > 1$  the tunneling density of states acquires a gap, as then the singlet character of the order parameter dominates.

In Fig. 10 (b) and (c), we show results for a hypothetical spin-orbit coupling of the form  $\mathbf{g} = \eta'[0, 0, \hat{k}_x \hat{k}_y \hat{k}_z (\hat{k}_x^2 - \hat{k}_y^2)]$ , that is consistent with the same point group symmetry  $D_{4v}$  as the Rashba spin-orbit coupling. For this case, a sharp zero bias conductance peak exists for  $q < 1$  in all tunneling directions. In contrast, for  $q > 1$ , the zero bias conductance peak only exists when tunneling perpendicular to the  $z$ -direction, however, not when tunneling parallel to the  $z$ -direction.

In Fig. 10 (d) we consider the cubic point group symmetry, and assume the simplest form of a fully isotropic spin-orbit interaction of the form  $\hat{\mathbf{g}} = [\hat{k}_x, \hat{k}_y, \hat{k}_z]$ . Here, for  $q < 1$  the tunneling conductance is zero at zero bias, but raises sharply away from

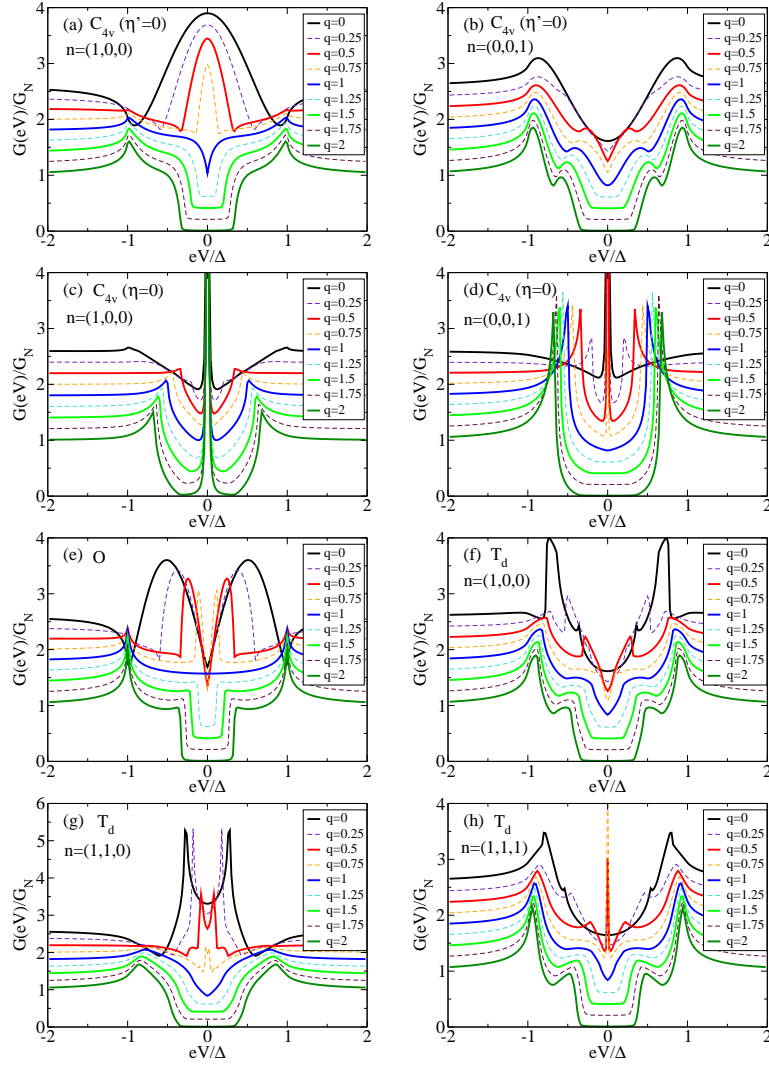


**Fig. 10** (Color online) Tunneling conductance  $G(eV)/G_N$  for various types of spin-orbit coupling corresponding to the indicated symmetry groups, and for various alignments of the surface normal  $\hat{n}$  as indicated. The spin-orbit vector is of the form  $C_{4v}$ :  $\mathbf{g} = \eta[\hat{k}_y, -\hat{k}_x, 0] + \eta'[0, 0, \hat{k}_x\hat{k}_y\hat{k}_z(\hat{k}_x^2 - \hat{k}_y^2)]$ ;  $O$ :  $\hat{\mathbf{g}} = [\hat{k}_x, \hat{k}_y, \hat{k}_z]$  (this case is fully isotropic);  $T_d$ :  $\hat{\mathbf{g}} = 2[\hat{k}_x(\hat{k}_y^2 - \hat{k}_z^2), \hat{k}_y(\hat{k}_z^2 - \hat{k}_x^2), \hat{k}_z(\hat{k}_x^2 - \hat{k}_y^2)]$ . The curves are for  $\Delta_{\pm} = \Delta_0(q \pm |\hat{\mathbf{g}}(\mathbf{k})|)/(q+1)$ , with  $q$  ranging from 0 to 2. The order parameter is assumed constant up to the surface, and a spherical Fermi surface with isotropic Fermi velocity is assumed. The tunneling parameter is  $D_0 = 0.1$ . Curves are vertically shifted by multiples of 0.2.

zero bias, showing side peaks due to Andreev bound states. At  $q = 1$  this structure disappears with only a pseudogap remaining. For  $q > 1$  a gap opens.

Finally, in Fig. 10 (e)-(g) we show results for the full tetrahedral point group  $T_d$ . We compare tunneling in (1,0,0), (1,1,0), and (1,1,1) directions. Note that in this case, the relation (107) between  $\mathbf{g}$  and  $\mathbf{k}$  is not invariant under a rotation of both vectors by 90 degree around the  $\hat{k}_x$ -,  $\hat{k}_y$ -, or  $\hat{k}_z$ -axis, but an overall sign change appears; however, the conductance spectra are insensitive to this sign change. For  $q < 1$  there is a vanishing zero bias conductance for tunneling in (1,0,0) direction, and a low-energy dispersive Andreev bound state branch for tunneling in (1,1,0) direction. For tunneling in (1,1,1) direction, the zero bias conductance vanishes for  $q = 0$ , and shows a sharp zero bias peak for  $0 < q < 1$ . For  $q > 1$  the tunneling conductance becomes gapped for all directions.

As can be seen from these results, studying directional resolved tunneling in non-centrosymmetric superconductors gives important clues about the order parameter symmetry and the type of spin-orbit interaction.

### 3.8.3 Andreev point contact spectra

Here we present results for the case of a point contact between a normal metal and a non-centrosymmetric superconductor. We use Eq. (80) to calculate the spectra, with a scattering matrix that has the form shown in Eq. (87). We assume isotropic Fermi surfaces in the materials on both sides of the interface, and for simplicity use equal magnitudes for Fermi momenta and velocities. The transmission amplitude is modeled by that for a  $\delta$ -function barrier,

$$t(\alpha_{\mathbf{k}}) = \frac{t_0 \cos(\alpha_{\mathbf{k}})}{\sqrt{1 - t_0^2 \sin^2(\alpha_{\mathbf{k}})}}, \quad (109)$$

and the component of the Fermi velocity along the interface normal in direction of current transport is  $\hat{\mathbf{n}}v_{F1} = v_F \cos(\alpha_{\mathbf{k}})$ .

In Fig. 11, the Andreev conductance  $G(eV)/G_N$  for various types of spin-orbit coupling and for various alignments of the surface normal  $\hat{\mathbf{n}}$  are shown. Here, the transmission probability  $D_0 = t_0^2$  is varied from zero to one. We restrict here to the case  $q = 0$ , i.e. an order parameter of the form  $\Delta_{\pm} = \pm \Delta_0 |\hat{\mathbf{g}}(\mathbf{k})|$ . Again, a spherical Fermi surface with isotropic Fermi velocity is assumed. We also compare the case of a surface layer with suppressed order parameter (dashed lines) with that of an order parameter constant up to the surface (full lines). To model the order parameter suppression, we assume a layer of thickness  $W = 2\xi_0$  with  $\xi_0 = \hbar v_F / 2\pi k_B T_c$  (dotted lines) in which the order parameter vanishes. Thus, we use Eq. (105) as incoming solutions for the coherence amplitudes. Note that for  $D_0 = 1$  the surface layer with zero order parameter does not affect the Andreev conductance. This is due to the fact that for perfect transmission the normal region simply extends slightly further towards the superconductor, and within our approximation we neglect the spin-orbit effects in interface potential.

For a larger spin-orbit coupling the interface between a normal metal and a normal conducting non-centrosymmetric metal with strong spin-orbit interaction becomes necessarily spin-active, as

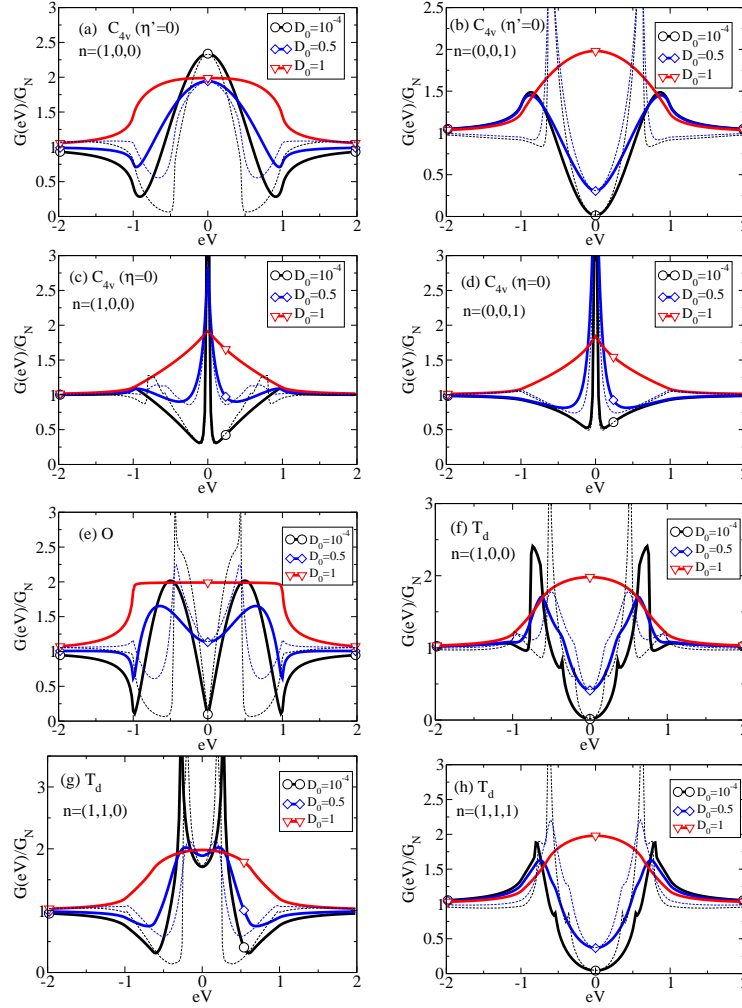


**Fig. 11** (Color online) Andreev conductance  $G(eV)/G_N$  for various types of spin-orbit coupling corresponding to the indicated symmetry groups and for the indicated alignments of the surface normal  $\hat{n}$ . The transmission probability  $D_0 = t_0^2$  is varied. The spin-orbit vector is of the form  $C_{4v}$ :  $\mathbf{g} = \eta[\hat{k}_y, -\hat{k}_x, 0] + \eta'[0, 0, \hat{k}_x\hat{k}_y\hat{k}_z(\hat{k}_x^2 - \hat{k}_y^2)]$ ;  $O$ :  $\mathbf{g} = [\hat{k}_x, \hat{k}_y, \hat{k}_z]$  (this case is fully isotropic);  $T_d$ :  $\mathbf{g} = 2[\hat{k}_x(\hat{k}_y^2 - \hat{k}_z^2), \hat{k}_y(\hat{k}_z^2 - \hat{k}_x^2), \hat{k}_z(\hat{k}_x^2 - \hat{k}_y^2)]$ . The curves are for  $\Delta_{\pm} = \pm\Delta_0|\hat{\mathbf{g}}(\mathbf{k})|$ . The order parameter is assumed constant up to the surface (full lines) or suppressed to zero in a surface layer of thickness  $W = 2\xi_0$  with  $\xi_0 = \hbar v_F/2\pi k_B T_c$  (dotted lines). For  $D_0 = 1$  these two cases give identical results. A spherical Fermi surface with isotropic Fermi velocity is assumed.

the interface potential term in the Hamiltonian must be hermitian. Thus, a perfect transmission is not realistic in such a case. For weak spin-orbit splitting these effects are also present, however modify the results only to order  $v_{SO}/E_F$ , or on energy scales  $v_{SO}^2/E_F$ .

For lower transmission, we remark as an overall observation that the suppression of the order parameter does not affect the value of the Andreev conductance at zero bias. This is simply due to the fact that in the clean limit the coherence amplitudes become effectively spatially constant for  $\varepsilon = 0$ . For higher bias, deviations can be observed, that in general lead to a shift of Andreev bound states to lower bias.

We turn now to the Andreev point contact spectra for  $t_0 = 1$ . As can be seen, the form of the spectrum is sensitive to the type of spin orbit coupling, and the associated order parameter symmetry. For a Rashba spin-orbit coupling, Fig. 11 (a) and (b), the Andreev conductance is enhanced to twice the normal conductance at zero bias, however to a smaller value for finite bias. There is a pronounced anisotropy in the shape of the Andreev conductance spectra. In (c) and (d) the Andreev conductance shows a sharp kink feature at zero bias, associated with the complex nodal structure of the spin-orbit vector. For cubic symmetry, (e), we observe an Andreev conductance resembling that of an *s*-wave spin singlet superconductor. And, finally, for a Dresselhaus spin-orbit coupling, (f)-(h), the Andreev conductance shows a behavior similar to the case of a Rashba spin-orbit interaction, however with a not so pronounced anisotropy.

## 4 Conclusions

We have given an overview over the current status of the theoretical understanding of Andreev bound states at the surface of a non-centrosymmetric superconducting material, and have presented results for tunneling conductance, point contact spectra, and spin polarized Andreev bound state spectra.

The new feature in non-centrosymmetric superconductors is the possible appearance of spin polarized Andreev states, that carry a spin-current along the interface or surface. The presence of such Andreev bound states that cross the chemical potential as a function of incident angle to the surface, is a topologically stable superconducting property. Such bound states exist as long as triplet order parameter components (in spin representation) dominate singlet components of the order parameter. When both components are equal, the bound states at the chemical potential disappears, and a topologically new ground state establishes. The transition between the two states is a quantum phase transition.

The spectrum of Andreev states at the surface provides valuable information about both the structure of the superconducting order parameter and the vector field of spin-orbit vectors on the Fermi surface. In this chapter we have concentrated on the rich structure that appears for the limiting case of a small spin-orbit splitting of the energy bands in the non-centrosymmetric material. In this limit, the spin quantum number is approximately conserved during scattering from surfaces and interfaces with normal metals, which leads to strong mixing between the helicity bands in the non-centrosymmetric material. The opposite limit of strong spin-orbit splitting is still largely unexplored. We have provided a theoretical basis in this chapter that allows to treat this case as well.

Finally, we would like to mention that interesting effects, like e.g. effects related to the spin Hall effect, or to Berry phases associated with the change of the spin-orbit vector along closed paths, are interesting subjects left for future studies.

**Acknowledgements** The authors would like to thank A. Balatsky, W. Belzig, J. Inoue, S. Kashiwaya, K. Kuroki, N. Nagaosa, J.A. Sauls, G. Schön, M. Sigrist, Y. Tanuma, I. Vekhter, A. Vorontsov, and T. Yokoyama for valuable discussions or contributions in connection with the topic of this chapter.

## References

1. I. Giaever, Phys. Rev. Lett. **5**, 147 (1960).
2. Y. Tanaka and S. Kashiwaya, Phys. Rev. Lett. **74**, 3451 (1995).
3. S. Kashiwaya and Y. Tanaka, Rep. Prog. Phys. **63**, 1641 (2000).
4. C. Bruder, Phys. Rev. B **41**, 4017 (1990).
5. C.R. Hu, Phys. Rev. Lett. **72**, 1526 (1994).
6. L.J. Buchholtz, M. Palumbo, D. Rainer, and J.A. Sauls, J. Low Temp. Phys. **101**, 1099 (1995).
7. L.J. Buchholtz and G. Zwicknagl, Phys. Rev. B **23** 5788 (1981); J. Hara and K. Nagai, Prog. Theor. Phys. **74** (1986) 1237.
8. C. Honerkamp and M. Sigrist, J. Low Temp. Phys. **111**, 895 (1998); M. Yamashiro, Y. Tanaka, and S. Kashiwaya, Phys. Rev. B **56**, 7847 (1997).
9. M. Matsumoto and M. Sigrist, J. Phys. Soc. Jpn. **68**, 994 (1999).
10. Y. Tanaka, T. Tanuma, K. Kuroki and S. Kashiwaya, J. Phys. Soc Jpn. **71** 2102 (2002).
11. J. Geerk, X.X. Xi, and G. Linker: Z. Phys. B. **73**, (1988), 329; S. Kashiwaya, Y. Tanaka, M. Koyanagi, H. Takashima, and K. Kajimura, Phys. Rev. B **51** (1995) 1350; L. Alff, H. Takashima, S. Kashiwaya, N. Terada, H. Ihara, Y. Tanaka, M. Koyanagi, and K. Kajimura, Phys. Rev. B **55**, (1997) R14757; M. Covington, M. Aprili, E. Paroanu, L.H. Greene, F. Xu, J. Zhu, and C.A. Mirkin, Phys. Rev. Lett. **79**, (1997) 277; J. Y. T. Wei, N.-C. Yeh, D. F. Garrigus and M. Strassik, Phys. Rev. Lett. **81**, (1998) 2542.
12. F. Laube, G. Goll, H. v. Löhneysen, M. Fogelström, and F. Lichtenberg, Phys. Rev. Lett. **84**, 1595 (2000).
13. Z.Q. Mao, K.D. Nelson, R. Jin, Y. Liu, and Y. Maeno, Phys. Rev. Lett. **87**, 037003 (2001); M. Kawamura, H. Yaguchi, N. Kikugawa, Y. Maeno, H. Takayanagi, J. Phys. Soc. Jpn. **74**, (2005) 531.
14. Ch. Wälti, H.R. Ott, Z. Fisk, and J.L. Smith, Phys. Rev. Lett. **84**, (2000) 5616.
15. P. M. C. Rourke, M. A. Tanatar, C. S. Turel, J. Berdeklis, C. Petrovic, and J. Y. T. Wei, Phys. Rev. Lett. **94**, (2005) 107005.
16. K. Ichimura, S. Higashi, K. Nomura and A. Kawamoto, Synthetic Metals Vol. 153 (2005) 409.
17. C.S. Turel, J.Y.T. Wei, W.M. Yuhasz and M.B. Maple, Physica C, 463-465 32 (2007).
18. Y. Aoki, Y. Wada, M. Saitoh, R. Nomura, Y. Okuda, Y. Nagato, M. Yamamoto, S. Higashitani, and K. Nagai, Phys. Rev. Lett. **95**, (2005) 075301.
19. G. E. Blonder, M. Tinkham, and T. M. Klapwijk, Phys. Rev. B **25**, 4515 (1982).
20. M. Eschrig, Phys. Rev. B **61**, 9061 (2000).
21. A. P. Mackenzie and Y. Maeno, Rev. Mod. Phys. **75**, (2003) 657; Y. Maeno et al., Nature **394**, 532 (1994)
22. Y. Maeno, H. Hashimoto, K. Yoshida, S. Nishizaki, T. Fujita, J. G. Bednorz, and F. Lichtenberg, Nature (London) **372**, 532 (1994).
23. K. Ishida, H. Mukuda, Y. Kitaoka, K. Asayama, Z. Q. Mao, Y. Mori, and Y. Maeno, Nature (London) **396**, 658 (1998).
24. G. M. Luke, Y. Fudamoto, K. M. Kojima, M. I. Larkin, J. Merrin, B. Nachumi, Y. J. Uemura, Y. Maeno, Z. Q. Mao, Y. Mori, H. Nakamura, and M. Sigrist, Nature (London) **394**, 558 (1998).



25. A. P. Mackenzie and Y. Maeno, *Rev. Mod. Phys.* **75**, 657 (2003).
26. K. D. Nelson, Z. Q. Mao, Y. Maeno, and Y. Liu, *Science* **306**, 1151 (2004); Y. Asano, Y. Tanaka, M. Sigrist, and S. Kashiwaya, *Phys. Rev. B* **67**, 184505 (2003); *Phys. Rev. B* **71**, 214501 (2005).
27. H. Kambara, S. Kashiwaya, H. Yaguchi, Y. Asano, Y. Tanaka and Y. Maeno, *Phys. Rev. Lett.* **101**, 267003 (2008).
28. Y. Tanuma, N. Hayashi, Y. Tanaka, and A. A. Golubov, *Phys. Rev. Lett.* **102**, 117003 (2009); T. Yokoyama, C. Iniotakis, Y. Tanaka, and M. Sigrist, *Phys. Rev. Lett.* **100**, 177002 (2008).
29. M. Fogelström, D. Rainer and J. A. Sauls, *Phys. Rev. Lett.* **79** 281 (1997).
30. F. Laube, G. Goll, M. Eschrig, M. Fogelström, and R. Werner, *Phys. Rev. B* **69**, 014516 (2004).
31. M. Yamashiro, Y. Tanaka, N. Yoshida, and S. Kashiwaya, *J. Phys. Soc. Jpn.* **68**, 2019 (1999).
32. See for e.g., *The Quantum Hall effect*, edited by R.E. Prange and S.M. Girvin, (Springer-Verlag, 1987), and references therein.
33. D. J. Thouless, M. Kohmoto, M. P. Nightingale, and M. den Nijs, *Phys. Rev. Lett.* **49**, 405 (1982).
34. J. Goryo and K. Ishikawa, *J. Phys. Soc. Jpn.* **67**, 3006 (1998); A. Furusaki, M. Matsumoto, and M. Sigrist, *Phys. Rev. B* **64** 054514 (2001).
35. E. Bauer, G. Hilscher, H. Michor, Ch. Paul, E.W. Scheidt, A. Gribanov, Yu. Seropegin, H. Noël, M. Sigrist, and P. Rogl, *Phys. Rev. Lett.* **92**, 027003 (2004).
36. P. A. Frigeri, D. F. Agterberg, A. Koga and M. Sigrist, *Phys. Rev. Lett.* **92**, 097001 (2004).
37. N. Reyren et al., *Science* **317**, 1196 (2007).
38. K. Yada, S. Onari, Y. Tanaka, and J. Inoue, *Phys. Rev. B* **80**, 140509 (2009).
39. X.L. Qi, T. L. Hughes, S. Raghu and S.C. Zhang, *Phys. Rev. Lett.* **102**, 187001 (2009); M. Sato and S. Fujimoto, *Phys. Rev. B* **79**, 094504 (2009); R. Roy, arXiv:cond-mat/0608064; C. K. Lu and S.-K. Yip *Phys. Rev. B* **78**, 132502 (2008); S.-K. Yip, arXiv:0910.0696.
40. Y. Tanaka, T. Yokoyama, A. V. Balatsky and N. Nagaosa, *Phys. Rev. B* **79**, 060505(R) (2009).
41. A. F. Andreev, *Sov. Phys. JETP* **19**, 1228 (1964).
42. C. Iniotakis, N. Hayashi, Y. Sawa, T. Yokoyama, U. May, Y. Tanaka, and M. Sigrist, *Phys. Rev. B* **76**, 012501 (2007).
43. T. Yokoyama, Y. Tanaka and J. Inoue, *Phys. Rev. B* **72** 220504(R) (2005).
44. A.B. Vorontsov, I. Vekhter, M. Eschrig, *Phys. Rev. Lett.* **101**, 127003 (2008).
45. J. Linder and A. Sudbø, *Phys. Rev. B* **76**, 054511 (2007).
46. K. Børkje and A. Sudbø, *Phys. Rev. B* **74**, 054506 (2006); K. Børkje, *Phys. Rev. B* **76**, 184513 (2007).
47. S. Kashiwaya, Y. Tanaka, N. Yoshida, and M.R. Beasley, *Phys. Rev. B*, **60** 3572 (1999).
48. M. König, S. Wiedmann, C. Brüne, A. Roth, H. Buhmann, L. Molenkamp, X.-L. Qi, and S.-C. Zhang, *Science*, **318**, 766 (2007).
49. C. L. Kane and E. J. Mele, *Phys. Rev. Lett.* **95**, 146802 (2005); C. L. Kane and E. J. Mele, *Phys. Rev. Lett.* **95**, 226801 (2005).
50. B. A. Bernevig, and S. C. Zhang, *Phys. Rev. Lett.* **96**, 106802 (2006).
51. L. Fu and C. L. Kane, *Phys. Rev. B* **74**, 195312 (2006); L. Fu and C. L. Kane, *Phys. Rev. B* **76**, 045302 (2007).
52. L. D. Landau, *Zh. Eksp. Teor. Fiz.* **32**, 59 (1957), [*Sov. Phys. JETP* **5**, 101 (1957)].
53. L. D. Landau, *Sov. Phys. JETP* **8**, 70 (1959).
54. J. W. Serene and D. Rainer, *Phys. Rep.* **101**, 221 (1983).
55. D. Rainer, in *Progress in Low Temperature Physics X*, p. 371, edited by D. F. Brewer (Elsevier Science Publishers, Amsterdam, 1986).
56. M. Eschrig, J. Heym, and D. Rainer, *J. Low Temp. Phys.* **95**, 323 (1994).
57. D. Rainer and J. A. Sauls, in *Superconductivity: From Basic Physics to New Developments*, edited by P. N. Butcher and Y. Lu (World Scientific, Singapore, 1995), pp. 45–78.
58. M. Eschrig, D. Rainer, and J.A. Sauls, *Phys. Rev. B* **59**, 12095 (1999); Appencix C.
59. A. I. Larkin and Y. N. Ovchinnikov, *Zh. Eksp. Teor. Fiz.* **55**, 2262 (1968), [*Sov. Phys. JETP* **28**, 1200 (1969)].
60. G. Eilenberger, *Z. Phys.* **214**, 195 (1968).

61. A. Schmid and G. Schön, *J. Low. Temp. Phys.* **20**, 207 (1975).
62. A. Schmid, in *Nonequilibrium Superconductivity, Phonons and Kapitza Boundaries*, Proceedings of NATO Advanced Study Institute, edited by K. E. Gray (Plenum Press, New York, 1981), Chapter 14.
63. J. Rammer and H. Smith, *Rev. Mod. Phys.* **58**, 323 (1986).
64. A. I. Larkin and Y. N. Ovchinnikov, in *Nonequilibrium Superconductivity*, edited by D. N. Langenberg and A. I. Larkin (Elsevier Science Publishers, 1986), p. 493.
65. M. Eschrig, J. A. Sauls, H. Burkhardt, and D. Rainer, in *High- $T_c$  Superconductors and Related Materials, Fundamental Properties, and Some Future Electronic Applications*, Proceedings of the NATO Advanced Study Institute, edited by S.-L. Drechsler and T. Mishonov, pp. 413-446 (Kluwer Academic, Norwell, MA, 2001).
66. L. P. Gor'kov, *Zh. Eksp. Teor. Fiz.* **34**, 735 (1958), [*Sov. Phys. JETP* **7**, 505 (1958)], L. P. Gor'kov, *Zh. Eksp. Teor. Fiz.* **36**, 1918 (1959), [*Sov. Phys. JETP* **9**, 1364 (1959)].
67. L. V. Keldysh, *Zh. Eksp. Teor. Fiz.* **47**, 1515 (1964), [*Sov. Phys. JETP* **20**, 1018 (1965)].
68. A. L. Shelankov, *J. Low. Temp. Phys.* **60**, 29 (1985).
69. J. A. Alexander, T. P. Orlando, D. Rainer, and P. M. Tedrow, *Phys. Rev. B* **31**, 5811 (1985).
70. M. Eschrig, J. A. Sauls, and D. Rainer, *Phys. Rev. B* **60**, 10447 (1999).
71. Y. Nagato, K. Nagai, and J. Hara, *J. Low Temp. Phys.* **93**, 33 (1993), S. Higashitani and K. Nagai, *J. Phys. Soc. Jpn.* **64**, 549 (1995), Y. Nagato, S. Higashitani, K. Yamada, and K. Nagai, *J. Low Temp. Phys.* **103**, 1 (1996).
72. N. Schopohl and K. Maki, *Phys. Rev. B* **52**, 490 (1995), N. Schopohl, cond-mat/9804064 (unpublished, 1998).
73. M. Eschrig, J. Kopu, A. Konstandin, J. C. Cuevas, M. Fogelström, and G. Schön, *Adv. in Sol. State Phys.* **44**, pp. 533-546, (Springer Verlag, Heidelberg, 2004).
74. J. C. Cuevas, J. Hammer, J. Kopu, J. K. Viljas, and M. Eschrig, *Phys. Rev. B* **73**, 184505 (2006).
75. A. L. Shelankov, *Sov. Phys. Solid State* **26**, 981 (1984) [*Fiz. Tved. Tela* **26**, 1615 (1984)].
76. A. V. Zaitsev, *Zh. Eksp. Teor. Fiz.* **86**, 1742 (1984) [*Sov. Phys. JETP* **59**, 1015 (1984)].
77. A. Millis, D. Rainer, and J. A. Sauls, *Phys. Rev. B* **38**, 4504 (1988).
78. S.-K. Yip, *J. Low Temp. Phys.* **109**, 547 (1997); C.-K. Lu and S.-K. Yip, *Phys. Rev. B* **80**, 024504 (2009).
79. M. Fogelström, *Phys. Rev. B* **62**, 11812 (2000).
80. A. Shelankov and M. Ozana, *Phys. Rev. B* **61**, 7077 (2000); A. Shelankov and M. Ozana, *J. Low Temp. Phys.* **124**, 223 (2001).
81. E. Zhao, T. Löfwander, and J.A. Sauls, *Phys. Rev. B* **70**, 134510 (2004).
82. M. Eschrig, *Phys. Rev. B* **80**, 134511 (2009).
83. R. Grein, M. Eschrig, G. Metalidis, and G. Schön, *Phys. Rev. Lett.* **102**, 227005 (2009).
84. M. Eschrig, J. Kopu, J. C Cuevas, and G. Schön, *Phys. Rev. Lett.* **90**, 137003 (2003).
85. J. Kopu, M. Eschrig, J. C. Cuevas, and M. Fogelström, *Phys. Rev. B* **69**, 094501 (2004).
86. M. Eschrig and T. Löfwander, *Nat. Phys.* **4**, 138 (2008).
87. T. Lück, P. Schwab, U. Eckern, and A. Shelankov, *Phys. Rev. B* **68**, 174524 (2003).
88. S. Graser and T. Dahm, *Phys. Rev. B* **75**, 014507 (2007).
89. P.A.Frigeri *et al.*, *Europ. Phys. Journ. B* **54**, 435 (2006).
90. I. A. Sergienko and S. H. Curnoe, *Phys. Rev. B* **70**, 213410 (2004).
91. N. Hayashi, K. Wakabayashi, P.A. Frigeri, and M. Sigrist, *Phys. Rev. B* **73**, 024504 (2006).
92. E. I. Rashba, *Phys. Rev. B* **68**, 241315 (2003).
93. E. G. Mishchenko, A. V. Shytov, and B. I. Halperin, *Phys. Rev. Lett.* **93**, 226602 (2004).